

Gravitational waves from extreme mass-ratio inspirals in Dynamical Chern-Simons gravity

Paolo Pani*

*CENTRA, Departamento de Física, Instituto Superior Técnico,
Universidade Técnica de Lisboa, Av. Rovisco Pais 1, 1049 Lisboa, Portugal*

Vitor Cardoso†

*CENTRA, Departamento de Física, Instituto Superior Técnico,
Universidade Técnica de Lisboa, Av. Rovisco Pais 1, 1049 Lisboa, Portugal and
Department of Physics and Astronomy, The University of Mississippi, University, MS 38677-1848, USA*

Leonardo Gualtieri‡

Dipartimento di Fisica, “Sapienza” Università di Roma and Sezione INFN Roma1, P.A. Moro 5, 00185, Roma, Italy

Dynamical Chern-Simons gravity is an interesting extension of General Relativity, which finds its way in many different contexts, including string theory, cosmological settings and loop quantum gravity. In this theory, the gravitational field is coupled to a scalar field by a parity-violating term, which gives rise to characteristic signatures. Here we investigate how Chern-Simons gravity would affect the quasi-circular inspiralling of a small, stellar-mass object into a large non-rotating supermassive black hole, and the accompanying emission of gravitational and scalar waves. We find the relevant equations describing the perturbation induced by the small object, and we solve them through the use of Green’s function techniques. Our results show that for a wide range of coupling parameters, the Chern-Simons coupling gives rise to an *increase* in total energy flux, which translates into a fewer number of gravitational-wave cycles over a certain bandwidth. For space-based gravitational-wave detectors such as LISA, this effect can be used to constrain the coupling parameter effectively.

PACS numbers: 04.50.Kd, 04.25.-g, 97.60.Lf, 04.30.-w

I. INTRODUCTION

The inspirals of stellar-mass compact objects, typically black holes (BHs) or neutron stars, into supermassive BHs at the galactic centers are among the most promising sources for the space-based gravitational wave detector LISA [1]. These processes are known as Extreme Mass-Ratio Inspirals (EMRIs) and allow for stringent tests of general relativity to be done, for several reasons [2, 3]. First of all, they emit 10^5 cycles or more of gravitational radiation in the LISA band, during the timespan of the LISA mission ($\sim 1-5$ years). Furthermore, this signal is emitted when the stellar mass object is close to the horizon of the supermassive BH, thus encoding the features of the strong-field BH spacetime and of the strong-curvature regime of general relativity [4]. Finally, EMRIs are expected to be relatively clean systems, with negligible perturbations from surrounding matter. Therefore, the detection of the signal from an EMRI would allow us to test the strong-field regime of gravity, where possible deviations from general relativity may show up. Of course, this would be possible only if we understand how alternative theories of gravity would affect the EMRI signal.

In this paper, we discuss the imprint on EMRI signals of dynamical Chern Simons (DCS) gravity, an extension of general relativity [5–8] in which the Einstein-Hilbert action is modified by adding a parity-violating Chern-Simons (CS) term, that couples gravity to a scalar field. Among other proposed alternative theories, there are strong motivations to consider DCS gravity. Indeed, this correction arises in many versions of string theory [9] and in loop quantum gravity [10–12]. Furthermore, CS gravity can be recovered as a truncation of low energy effective string models [8, 13] and could also explain several problems in cosmology [14–18] (see Ref. [19] for a recent review).

DCS gravity would affect the EMRI signal in several ways. First of all, it modifies the spacetime metric of rotating BHs [20] (though the metric of spherical, stationary BHs is not affected). These modifications induce deviations in the motion of the stellar mass object, which affect the emitted gravitational signal. This effect has been studied in [21], where the deviation of EMRI orbits due to spacetime metric modification has been evaluated. In addition, in this theory the dynamical equations of gravity change, as the gravitational field is coupled with a scalar field. This is the effect studied in this paper, in which we evaluate the change of the EMRI signal due to the DCS modification of the dynamical equations of the gravitational field.

We shall focus on the simplest case of EMRI system: the inspiralling of a test particle around a Schwarzschild

* paolo.pani@ist.utl.pt

† vitor.cardoso@ist.utl.pt

‡ leonardo.gualtieri@roma1.infn.it

BH. Since the Schwarzschild metric is a solution of DCS gravity, the orbital effects studied in [21] vanish. However, as we will show, DCS gravity could significantly affect the EMRI signal. We generalize the equations describing perturbations of Schwarzschild DCS BHs, derived previously by some of us [22, 23], to include a source term describing an orbiting particle. Then, we solve these equations using a generalization of the Green's function method, evaluating the emitted flux of gravitational energy and scalar energy. Finally, we determine how the modified energy loss affects the emitted gravitational signal, by computing the change in the number of orbital cycles. Similar methods have been already successfully applied to study the effects of neutron star structure in EMRI systems [24], to investigate the nature of the central massive object [25] and also to put constraints on other alternative theories of gravity, like Brans-Dicke theory [26].

We find that, although the DCS coupling only mildly changes the total energy flux, the corrections accumulate during the EMRI inspiral, producing a decrease $\delta\mathcal{N}$ in the number of orbital cycles which is potentially detectable by LISA. Our results can be summarized by the following fit:

$$\delta\mathcal{N} \sim -26\zeta\sqrt{\frac{M_\odot}{m_2}} \exp\left\{-1.2\log_{10}\left[\frac{m_1}{m_{\max}}\right]\right\}, \quad (1.1)$$

where $m_{\max} \sim 10^6 M_\odot$ (its precise definition is given in Eq. (4.21)), ζ is a parameter characterizing the DCS correction, and m_1, m_2 are the masses of the supermassive BH and of the stellar mass object, respectively. The fit above is valid in a wide region of the parameter space, i.e. $m_1 \in [10^5, 10^7] M_\odot$, $m_2 \in [1, 10] M_\odot$ and $\zeta \leq 1$, with an error of at most a few percent. For larger values of ζ , the fit (1.1) still gives an order-of-magnitude estimate of $\delta\mathcal{N}$: for $1 \leq \zeta \leq 20$, the error does not exceed 50%.

The plan of the paper is the following. In Section II we discuss the equations describing perturbations of the Schwarzschild metric in DCS gravity induced by a point-like particle on a circular orbit about the BH. In Section III we describe the Green's function approach to solve the perturbation equations. In Section IV A we derive the energy flux associated to the gravitational and scalar radiation, and compute this flux solving numerically the perturbation equations. In Section IV B we determine how this energy flux affects the gravitational signal. In Section V we draw our conclusions. The derivation of the perturbation equations with source is discussed in detail in Appendix A. Appendix B is devoted to describe a perturbative Green's function approach, which is valid in the small coupling limit and may be potentially useful for future analytical calculations. In Appendix C we compare different prescriptions to compute the number of orbital cycles.

II. DCS GRAVITY AND PERTURBATION EQUATIONS

The action of DCS gravity reads [20] (we use geometrical units $c = G = 1$)

$$S = \frac{1}{16\pi} \int d^4x \sqrt{-g} R + \frac{\alpha}{4} \int d^4x \sqrt{-g} \vartheta^* R R - \frac{\beta}{2} \int d^4x \sqrt{-g} [g^{ab} \nabla_a \vartheta \nabla_b \vartheta + V(\vartheta)] + S_{\text{mat}}, \quad (2.1)$$

where ϑ is the scalar field and

$$*RR = R_{abcd} *R^{abcd} = \frac{1}{2} R_{abcd} \epsilon^{baef} R_{ef}^{cd}. \quad (2.2)$$

Neglecting the scalar potential $V(\vartheta)$, the equations of motion are

$$R_{ab} = -16\pi\alpha C_{ab} + 8\pi \left(T_{ab} - \frac{1}{2} g_{ab} T \right) \quad (2.3)$$

$$\square\vartheta = -\frac{\alpha}{4\beta} *RR \quad (2.4)$$

where the stress-energy tensor accounts for the matter and the scalar field contributions, $T_{ab} = T_{ab}^{\text{mat}} + T_{ab}^\vartheta$, with

$$T_{ab}^\vartheta = \beta \left(\vartheta_{;a} \vartheta_{;b} - \frac{1}{2} \vartheta_{;c} \vartheta^{;c} \right), \quad (2.5)$$

and

$$C^{ab} = \vartheta_{;c} \epsilon^{cde} (a \nabla_e R^b)_d + \vartheta_{;dc} *R^{d(ab)c}. \quad (2.6)$$

Since in any spherically symmetric background $*RR \equiv 0$ and $C^{ab} \equiv 0$, spherically symmetric solutions of general relativity, like the Schwarzschild metric

$$ds^2 = -f dt^2 + f^{-1} dr^2 + r^2 d\Omega^2, \quad (2.7)$$

are solutions of DCS gravity [19]. Here, M is the ADM mass of the spacetime and

$$f = 1 - 2M/r. \quad (2.8)$$

A remarkable feature of EMRIs is that they can be described with great accuracy within a perturbative approach and in an adiabatic approximation. Indeed, during most of the inspiral the stellar-mass object can be considered as a test particle moving in a single massive BH background, the timescale for merger being much longer than a single orbital period. Hence, at each instant, we consider that the particle follows a geodesic of the BH spacetime and the geodesic parameters, i.e. the orbital energy and angular momentum of the particle, would change *adiabatically*: they can be computed by solving the linearized Einstein's equations for geodesic motion. In this way one finds the inspiralling orbit and the corresponding gravitational waveform, as explained below. This procedure takes into account the main effect of the back-reaction (the so-called “non-conservative part of the self-force”). A more detailed analysis, which would

also consider the “conservative part of the self-force” (see [27, 28] for the case of non-rotating BHs and [29, 30] for a review), is beyond the scope of this work.

Remarkably, due to Eq. (2.4), the tensor (2.6) satisfies $\nabla^a C_{ab} = 8\pi \nabla^a T_{ab}^\vartheta$. Using the latter equation and the Bianchi identities, the matter stress-energy tensor is conserved also in DCS gravity, i.e. $\nabla^a T_{ab}^{\text{mat}} = 0$. It follows that point-like particles travel on geodesics, exactly as in general relativity. Furthermore, we assume that the point-particle is non-spinning, neglecting the effects of spin-orbit interactions. These effects are proportional to the mass-ratio and they can be safely neglected in the study of EMRI systems [31].

We shall study the perturbations of a static, spherically symmetric BH of mass M , due to a non-spinning point-like particle of mass μ on a circular orbit around the BH. As discussed in [23], the Schwarzschild metric (2.7) with a vanishing scalar field is the only static, spherically symmetric BH solution in DCS gravity. In this background, we expand the gravitational and scalar perturbations induced by a point-like particle in tensor spherical harmonics, building the Zerilli and Regge-Wheeler functions, $Z^{\ell m}(r)$, $Q^{\ell m}(r)$, and the scalar field function $\Theta^{\ell m}(r)$. In the frequency domain, the perturbation equations read (see Appendix A for details):

$$\left[\frac{d^2}{dr_*^2} + \omega^2 - V_{RW}(r) \right] Q^{\ell m}(r) = T_{RW}(r) \Theta^{\ell m}(r) + S_{RW}^{\ell m}(r) \quad (2.9)$$

$$\left[\frac{d^2}{dr_*^2} + \omega^2 - V_S(r) \right] \Theta^{\ell m}(r) = T_S(r) Q^{\ell m}(r) + S_S^{\ell m}(r) \quad (2.10)$$

$$\left[\frac{d^2}{dr_*^2} + \omega^2 - V_Z(r) \right] Z^{\ell m}(r) = S_Z^{\ell m}(r). \quad (2.11)$$

In the equations above r_* is the tortoise coordinate defined by $dr/dr_* = f$, and the potentials read

$$V_{RW}(r) = f \left(\frac{\ell(\ell+1)}{r^2} - \frac{6M}{r^3} \right) \quad (2.12)$$

$$T_{RW}(r) = f \frac{96i\pi M\omega\alpha}{r^5} \quad (2.13)$$

$$V_S(r) = f \left(\frac{\ell(\ell+1)}{r^2} \left[1 + \frac{576\pi M^2\alpha^2}{r^6\beta} \right] + \frac{2M}{r^3} \right) \quad (2.14)$$

$$T_S(r) = -f \frac{(\ell+2)!}{(\ell-2)!} \frac{6M i \alpha}{r^5 \beta \omega} \quad (2.15)$$

$$V_Z(r) = \frac{f}{r^2 \Lambda^2} \left[2\lambda^2 \left(\lambda + 1 + \frac{3M}{r} \right) + \frac{18M^2}{r^2} \left(\lambda + \frac{M}{r} \right) \right], \quad (2.16)$$

where $\lambda = (\ell+2)(\ell-1)/2$ and $\Lambda = \lambda + 3M/r$. The source terms are given in Appendix A: $S_{RW}^{\ell m}$ and $S_Z^{\ell m}$ (cf. Eqs. (A10) and (A14)) are the same as those computed in general relativity [32], whereas $S_S^{\ell m}$ (cf. Eq. (A12)) is proportional to α and it is a novel term introduced by the CS coupling.

We stress that Eqs. (2.9) and (2.10) are coupled through the CS coupling α . In the sourceless case (i.e., no exterior matter), they reduce to those in Refs. [22, 23] with $Q^{\ell m} = i\omega \Psi^{\ell m}$ (notice the sign difference due to our definition (A8)). In the general relativity limit $\alpha = 0$, they decouple into the Regge-Wheeler equation with sources [32, 33] plus Klein-Gordon equation without source. Interestingly, in the DCS Schwarzschild background the polar (even parity) gravitational sector, Eq. (2.11), decouples from the scalar sector. Thus the CS coupling does not affect the Zerilli equation, which simply reads as in general relativity [32].

To conclude this Section, we remark that if we rescale the scalar field, in order to express its kinetic term in a canonical form

$$\theta \rightarrow \frac{\theta}{\sqrt{\beta}}, \quad (2.17)$$

then the DCS action takes the form

$$S = \frac{1}{16\pi} \int d^4x \sqrt{-g} R + \frac{\sqrt{\xi}}{16\sqrt{\pi}} \int d^4x \sqrt{-g} \vartheta^* R R - \frac{1}{2} \int d^4x \sqrt{-g} \left[g^{ab} \nabla_a \vartheta \nabla_b \vartheta + \tilde{V}(\vartheta) \right] + S_{\text{mat}}, \quad (2.18)$$

where, following Ref. [20], we have defined $\xi \equiv 16\pi\alpha^2/\beta$. Therefore, we expect that all physical observables depend on the parameter ξ (see also the discussion in [20]), or equivalently on the dimensionless parameter

$$\zeta = \frac{16\pi\alpha^2}{\beta M^4} = \frac{\xi}{M^4}, \quad (2.19)$$

where M is a quantity with the dimensions of mass (i.e. of length) associated to the system under consideration (in our case, the mass of the supermassive BH). This is indeed the case, as we shall show, for the motion of a test particle around a static, spherically symmetric BH. This procedure, of rescaling the scalar field to have a canonical kinetic term in order to get rid of redundant parameters, is well known in the context of scalar-tensor theories (see [34] and references therein). However, here we shall follow the formulation of Ref. [20], where α and β are kept as independent parameters.

III. GREEN'S FUNCTION APPROACH

In order to compute the gravitational-wave emission of a particle in geodesic motion around a spherically symmetric BH in DCS gravity, we shall solve the equations (2.9)-(2.11) by extending the standard Green's function techniques. As explained below, we work out the basic equations for general orbits, and then we specialize to circular motion. Our results can be easily generalized to eccentric orbits. In Appendix B we develop a perturbative approach, which is valid in the small-coupling limit, and we compare it with the general method discussed in this section (the agreement is very good for small coupling).

A. Even sector

We start by considering the Zerilli equation (2.11), which is not modified in DCS gravity. One considers two solutions $Z_{\pm}^{\ell m}$ of the associate homogeneous equation

$$\left[\frac{d^2}{dr_*^2} + \omega^2 - V_Z \right] Z_{\pm} = 0, \quad (3.1)$$

(hereafter, we leave implicit the ℓ, m indices) such that

$$Z_{\pm} \rightarrow e^{\pm i\omega r_*}, \quad r_* \rightarrow \pm\infty. \quad (3.2)$$

Then the general solution reads

$$Z(r) = \frac{1}{W_Z} \left[Z_+(r) \int_{-\infty}^r dr_* Z_- S_Z + Z_-(r) \int_r^{+\infty} dr_* Z_+ S_Z \right], \quad (3.3)$$

where $W_Z \equiv f(Z_- Z'_+ - Z_+ Z'_-)$ is the Wronskian and the prime denotes derivative with respect to the Schwarzschild radial coordinate, r . At infinity and at the horizon, where the energy flux is computed in term of Z , we get

$$Z(r_* \rightarrow \pm\infty) = \frac{e^{\pm i\omega r_*}}{W_Z} \int_{-\infty}^{\infty} dr_* Z_{\mp} S_Z. \quad (3.4)$$

As we show in Appendix A, for a circular orbit at $r = \bar{r}$ the source term has the form $S_Z \sim \delta(r - \bar{r})$. In this case to compute the integral (3.4) it is sufficient to evaluate the integrand at $r = \bar{r}$.

B. Odd sector

Let us consider the modified Regge-Wheeler equation (2.9), coupled with the scalar equation (2.10):

$$\begin{aligned} \left[\frac{d^2}{dr_*^2} + \omega^2 - V_{RW} \right] Q &= S_{RW} + \frac{96i\pi M\omega f}{r^5} \alpha \Theta, \quad (3.5) \\ \left[\frac{d^2}{dr_*^2} + \omega^2 - V_S \right] \Theta &= S_S - f \frac{(\ell+2)!}{(\ell-2)!} \frac{6iM\alpha}{\omega r^5 \beta} Q. \end{aligned} \quad (3.6)$$

Introducing $P^{\ell m} = dQ^{\ell m}/dr_*$ and $\Phi^{\ell m} = d\Theta^{\ell m}/dr_*$, we can write the equations above as a first order system

$$\frac{d\Psi}{dr_*} + V\Psi = \mathbf{S}, \quad (3.7)$$

where $\Psi = (Q, \Theta, P, \Phi)^T$ and $\mathbf{S} = (0, 0, S_{RW}, S_S)^T$ are four dimensional vectors and V reads

$$V = \begin{pmatrix} 0 & 0 & -1 & 0 \\ 0 & 0 & 0 & -1 \\ \omega^2 - V_{RW} & -T_{RW} & 0 & 0 \\ -T_S & \omega^2 - V_S & 0 & 0 \end{pmatrix}. \quad (3.8)$$

The system (3.7) can be solved by standard methods (see e.g. Ref. [35]). For this purpose, define the 4×4 matrix

X whose n th column contains the n th solution of the homogeneous system $d\mathbf{x}/dr_* + V\mathbf{x} = 0$, i.e. $X_{ij} = x_i^{(j)}$, where the j index denotes a solution of the homogeneous system and i is the vector index. It can be shown that also the matrix X constructed in such a way is a solution of the associated homogeneous system, in the sense that

$$\frac{dX}{dr_*} + VX = 0. \quad (3.9)$$

In order to solve (3.7), we impose the ansatz $\Psi = X\Xi$, where Ξ is a vector to be determined. Substituting the equation above into the inhomogeneous system and using Eq. (3.9) we find

$$\frac{d\Xi}{dr_*} = X^{-1}\mathbf{S}, \quad (3.10)$$

and the solution to (3.7) reads

$$\Psi = X \int dr_* X^{-1}\mathbf{S}. \quad (3.11)$$

The matrix X , contains four independent solutions of the homogeneous system, supplied by suitable boundary conditions. We impose

$$\begin{pmatrix} Q \\ \Theta \end{pmatrix} \rightarrow \begin{pmatrix} A_{\pm} \\ B_{\pm} \end{pmatrix} e^{\pm i\omega r_*}, \quad r_* \rightarrow \pm\infty. \quad (3.12)$$

As explained in Ref. [23], two linear independent solutions can be constructed by choosing: (i) $A_{\pm} = 1$ and an arbitrary $B_{\pm} = B_{\pm}^{(0)}$ and (ii) $B_{\pm} = 1$ and an arbitrary $A_{\pm} = A_{\pm}^{(0)}$, provided $A_{\pm}^{(0)} B_{\pm}^{(0)} \neq 1$. This procedure can be applied twice: first we construct two solutions, $\{\mathbf{x}_-^{(1)}, \mathbf{x}_-^{(2)}\}$, imposing boundary conditions at the horizon and integrating outward, and secondly we construct two further independent solutions, $\{\mathbf{x}_+^{(1)}, \mathbf{x}_+^{(2)}\}$, by imposing boundary conditions at infinity and integrating backward.

Finally, from Eq. (3.11), we can write the solutions for the gravitational and scalar waveform, which satisfy the correct boundary conditions, as follows

$$Q(r) = \sum_{i=1}^2 \left(Q_+^{(i)}(r) I_-^{(i)}(r) + Q_-^{(i)}(r) I_+^{(i)}(r) \right), \quad (3.13)$$

$$\Theta(r) = \sum_{i=1}^2 \left(\Theta_+^{(i)}(r) I_-^{(i)}(r) + \Theta_-^{(i)}(r) I_+^{(i)}(r) \right), \quad (3.14)$$

where

$$I_{\pm}^{(i)} = \int_{\pm\infty}^r dr_* \left(C_{\pm}^{(i)} S_{RW} + D_{\pm}^{(i)} S_S \right), \quad (i = 1, 2)$$

and the functions $C_{\pm}^{(i)}$ and $D_{\pm}^{(i)}$ depend on the solutions of the homogeneous system, $\{\mathbf{x}_-^{(1)}, \mathbf{x}_-^{(2)}\}$ and $\{\mathbf{x}_+^{(1)}, \mathbf{x}_+^{(2)}\}$, and can be straightforwardly computed from the components of the vector $X^{-1}\mathbf{S}$. For completeness, their expressions are given in Appendix D.

C. Circular orbits

So far our approach generically holds for a point-like particle in geodesic motion. However, the above formulae simplify significantly in the case of circular geodesics at $r = \bar{r}$, as we show in Appendix A. In particular, the source term for the scalar equation vanishes, $S_s \equiv 0$. The remaining source terms can be factorized in order to extract a Dirac delta contribution $\sim \delta(\omega - m\omega_K)$, where ω_K is the Keplerian frequency (A26). In the rest of this Section we write explicitly the indices ℓ, m and the dependence on ω .

To compute the Zerilli function we replace Eq. (A33) in Eq. (3.3). Integrating by parts to get rid of the derivative of the delta function, we get $Z_{\pm}^{\ell m}(\omega, r) = \bar{Z}_{\pm}^{\ell m}(r)\delta(\omega - m\omega_K)$ with

$$\bar{Z}_{\pm}^{\ell m}(r) = \frac{Z_{\mp}(r)}{W_Z} \left[\frac{Z_{\pm} \hat{G}_Z^{\ell m}}{f} - \left(\frac{Z_{\pm} \hat{F}_Z^{\ell m}}{f} \right)' \right]_{\bar{r}},$$

for $r \leq \bar{r}$ respectively; hatted quantities are defined in Appendix A, to which we refer for further details. At the boundaries, if we call $\mathcal{Z}_{\pm}^{\ell m}(\omega) \equiv Z_{\pm}^{\ell m}(\omega, r_* \rightarrow \pm\infty)$, we obtain

$$\mathcal{Z}_{\pm}^{\ell m}(\omega) = \frac{1}{W_Z} \left[\frac{Z_{\mp} \hat{G}_Z^{\ell m}}{f} - \left(\frac{Z_{\mp} \hat{F}_Z^{\ell m}}{f} \right)' \right]_{\bar{r}} \delta(\omega - m\omega_K) e^{\pm i\omega r_*}.$$

For later use, we will write this as

$$\mathcal{Z}_{\pm}^{\ell m}(\omega) = \bar{\mathcal{Z}}_{\pm}^{\ell m} \delta(\omega - m\omega_K) e^{\pm i\omega r_*}, \quad (3.15)$$

where $\bar{\mathcal{Z}}_{\pm}^{\ell m}$ is a constant.

A similar procedure can be applied to the axial sector. Using Eq. (A32), the Fourier transform of the Regge-Wheeler and scalar function, at the boundary $r_* \rightarrow \pm\infty$, read

$$\mathcal{Q}_{\pm}^{\ell m}(\omega) = \bar{\mathcal{Q}}_{\pm}^{\ell m} \delta(\omega - m\omega_K) e^{\pm i\omega r_*} \quad (3.16)$$

$$\Theta_{\pm}^{\ell m}(\omega) = \bar{\Theta}_{\pm}^{\ell m} \delta(\omega - m\omega_K) e^{\pm i\omega r_*}, \quad (3.17)$$

where, from Eqs. (3.13) and (3.14), we have

$$\begin{aligned} \bar{\mathcal{Q}}_{\pm}^{\ell m} &= \left\{ A_{\pm}^{(1)} \left[\frac{C_{\pm}^{(1)} G_{RW}}{f} - \left(\frac{C_{\pm}^{(1)} F_{RW}}{f} \right)' \right]_{\bar{r}} + \right. \\ &\quad \left. + A_{\pm}^{(2)} \left[\frac{C_{\pm}^{(2)} G_{RW}}{f} - \left(\frac{C_{\pm}^{(2)} F_{RW}}{f} \right)' \right]_{\bar{r}} \right\}, \\ \bar{\Theta}_{\pm}^{\ell m} &= \left\{ B_{\pm}^{(1)} \left[\frac{C_{\pm}^{(1)} G_{RW}}{f} - \left(\frac{C_{\pm}^{(1)} F_{RW}}{f} \right)' \right]_{\bar{r}} + \right. \\ &\quad \left. + B_{\pm}^{(2)} \left[\frac{C_{\pm}^{(2)} G_{RW}}{f} - \left(\frac{C_{\pm}^{(2)} F_{RW}}{f} \right)' \right]_{\bar{r}} \right\}. \end{aligned}$$

As we show in the next section, the energy flux at infinity and at the horizon can be computed in terms of the quantities $\mathcal{Z}_{\pm}^{\ell m}$, $\mathcal{Q}_{\pm}^{\ell m}$ and $\Theta_{\pm}^{\ell m}$ given in Eqs. (3.15), (3.16) and (3.17), respectively.

IV. RESULTS

A. Energy flux

The flux of gravitational energy can be computed in terms of metric perturbations. At asymptotically flat, future, null infinity, the expressions of the effective gravitational wave stress-energy tensor (i.e. the Isaacson tensor) in DCS gravity and in general relativity coincide [36]. Therefore, we can use the machinery derived in the framework of general relativity to determine the emitted gravitational energy flux at infinity in DCS gravity.

On the other hand, the expression of the rate of energy absorbed by the horizon is also formally equivalent to that in general relativity (see e.g. Ref. [37]). Indeed, the derivation involves the first law of BH thermodynamics, which relates the change in energy \dot{M} with the change in the horizon area \dot{A} , and Raychaudhuri's equation to calculate \dot{A} in terms of the shear tensor. In DCS gravity, both these steps proceed exactly as in general relativity, all the dynamical information being eventually encoded in the waveforms.

Hence, the energy fluxes at (null) infinity and at the horizon formally read as in general relativity [38]

$$\begin{aligned} \dot{E}_{grav}^{\pm} &\equiv \left\langle \frac{dE_{grav}}{dx} \right\rangle \\ &= \frac{1}{64\pi} \frac{(\ell+2)!}{(\ell-2)!} \sum_{\ell m} \left[|\dot{\mathcal{Z}}_{\pm}^{\ell m}(x)|^2 + 4|\mathcal{Q}_{\pm}^{\ell m}(x)|^2 \right], \end{aligned} \quad (4.1)$$

where the sum is taken over negative and positive m and $x = t \mp r_*$ are the retarded and advanced coordinates, respectively. The inverse Fourier transform of (3.15), (3.16) is

$$\begin{aligned} \mathcal{Z}_{\pm}^{\ell m}(t \mp r_*) &= \int d\omega \bar{\mathcal{Z}}_{\pm}^{\ell m} \delta(\omega - m\omega_K) e^{-im\omega_K(t \mp r_*)} \\ &= \bar{\mathcal{Z}}_{\pm}^{\ell m} e^{-im\omega_K(t \mp r_*)} \\ \mathcal{Q}_{\pm}^{\ell m}(t \mp r_*) &= \int d\omega \bar{\mathcal{Q}}_{\pm}^{\ell m} \delta(\omega - m\omega_K) e^{-im\omega_K(t \mp r_*)} \\ &= \bar{\mathcal{Q}}_{\pm}^{\ell m} e^{-im\omega_K(t \mp r_*)}, \end{aligned}$$

therefore

$$\dot{E}_{grav}^{\pm} = \frac{1}{64\pi} \frac{(\ell+2)!}{(\ell-2)!} \sum_{\ell m} \left[(m\omega_K)^2 |\bar{\mathcal{Z}}_{\pm}^{\ell m}|^2 + 4|\bar{\mathcal{Q}}_{\pm}^{\ell m}|^2 \right]. \quad (4.2)$$

On the other hand, the scalar energy flux reads (see, e.g. Ref. [32])

$$\dot{E}_{scal} = -r^2 f(r) \int d\Omega T_{tr}^{scal}. \quad (4.3)$$

From the stress-energy tensor of the scalar field, $T_{ab}^{scal} = \beta(\nabla_a \vartheta^* \nabla_b \vartheta - 1/2 g_{ab} \nabla_c \vartheta \nabla^c \vartheta^*)$. Inserting Eq. (A1) and

using the asymptotic behavior at infinity (3.17), the energy flux reads

$$\dot{E}_{scal}^{\pm} \equiv \left\langle \frac{dE_{scal}}{dx} \right\rangle = \sum_{\ell m} (m\omega_K)^2 \beta |\bar{\Theta}_{\pm}^{\ell m}|^2. \quad (4.4)$$

Finally, since the orbital frequency is related to the orbital velocity v and to the semi-latus rectum (which for circular orbits is simply $p = \bar{r}/M$) by the relations

$$v = (M\omega_K)^{1/3} = p^{-1/2}, \quad (4.5)$$

the energy flux \dot{E} can also be considered either as a function of v or p . The condition for the existence of stable circular orbits, $\bar{r} > r_{\text{ISCO}} = 6M$, constrains the values of v and p to $p > 6$ and $v < 6^{-1/2} \sim 0.408$.

The method described above has been implemented in MATHEMATICA. In our numerical approach, we have considered a series expansion at the horizon and at infinity up to order eight for the boundary conditions (3.2) and (3.12). Our results are summarized in Fig. 1. When $\zeta = 0$, our results agree with those in general relativity [39, 40] within one part in 10^6 or better. Furthermore, in the small ζ limit, we develop an independent method (discussed in Appendix B) whose results are in perfect agreement with the ones discussed here.

As expected, the CS corrections are more effective when $p \sim 6$, i.e. close to the innermost stable circular orbit (ISCO), where circular orbits probe the strong curvature region around the massive BH. Far away from the source the CS contributions are negligible. This is clear from the left panel of Fig. 1, where we show the relative difference in the emitted power

$$\frac{\delta \dot{E}}{\dot{E}_{\text{GR}}} \equiv \frac{\dot{E}_{\text{DCS}} - \dot{E}_{\text{GR}}}{\dot{E}_{\text{GR}}}, \quad (4.6)$$

where $\dot{E}_{\text{DCS}} = \dot{E}_{\text{grav}}^H + \dot{E}_{\text{grav}}^{\infty} + \dot{E}_{\text{scal}}^H + \dot{E}_{\text{scal}}^{\infty}$, i.e. it is the sum of the contributions coming from the gravitational and scalar fluxes, both at the infinity and the horizon, and $\dot{E}_{\text{GR}} = \dot{E}_{\text{DCS}}(\zeta = 0)$, i.e. the energy flux in general relativity. Clearly, the scalar contribution to \dot{E}_{GR} is vanishing. The relative difference is positive, i.e. the total power emitted in DCS gravity is *larger* than in general relativity. This is consistent with the fact that in this theory there is an extra scalar degree of freedom, which introduces further energy dissipation channels. Although the difference in the *total* flux is positive, we find that for some subdominant ($\ell \geq 3$) mode, the energy flux may be smaller than the corresponding flux in general relativity. This shows that a conversion of scalar into gravitational energy is possible, due to the CS coupling.

Furthermore, even if the axial flux can be as large as twice the axial flux in general relativity (for example when $p \sim 6$ and for $\zeta \sim 10$), the correction to the total energy flux is significantly smaller. Indeed, the leading contribution to the energy flux arises from $\ell = m$ modes, which have polar parity because selection rules

imply that for even values of $\ell + m$ only polar perturbations are sourced (see Appendix A for details). Therefore, since DCS corrections only affect the axial sector of Schwarzschild perturbations, their contribution is subleading with respect to that coming from the polar perturbations. In the most favorable case ($p \sim 6$ and $\zeta \sim 10$) the total energy flux (summing over polar and axial contributions up to $\ell = 5$ and $-l \leq m \leq l$) only differs from the general relativity value by a few percent. Typically, the deviation is smaller, as shown in the left panel of Fig. 1.

In the right panel of Fig. 1 we show the four contributions to the total emitted power. Remarkably, the main contributions arise from the gravitational and scalar flux *at the horizon*, which are positive and sensibly larger than the contributions at infinity; see Appendix B for a discussion on this behaviour.

Note that the correction to the gravitational flux at infinity is negative but, since this is a subleading contribution, the correction to the total energy flux is nevertheless positive.

Finally, from the results shown in Fig. 1 we can extract the following dependence in the small v limit

$$\frac{\delta \dot{E}_{\text{grav}}^H}{\dot{E}_{\text{GR}}^{\text{tot}}} \sim v^{10}, \quad \frac{\delta \dot{E}_{\text{scal}}^H}{\dot{E}_{\text{GR}}^{\text{tot}}} \sim v^{10}, \quad (4.7)$$

$$\frac{\delta \dot{E}_{\text{grav}}^{\infty}}{\dot{E}_{\text{GR}}^{\text{tot}}} \sim v^{12}, \quad \frac{\delta \dot{E}_{\text{scal}}^{\infty}}{\dot{E}_{\text{GR}}^{\text{tot}}} \sim v^{14}. \quad (4.8)$$

Notice that the high power in v introduces large errors in the fits above and these results should be understood as *lower limits* for the post-Newtonian (PN) orders of the CS effects. The scalar flux at infinity is consistent with analytical predictions at PN level [41].

B. Gravitational-wave signal

Although the difference between the energy emission by EMRIs in general relativity and their emission in DCS gravity is small, stellar-mass objects can orbit supermassive BHs for $\sim 10^5$ cycles (many of which can occur near the ISCO) while in the sensitivity window of LISA, before reaching the ISCO and eventually plunge. Hence, the small deviations accumulate and they can result in sensible modifications when one looks at the entire inspiral+merger process. Let us give a rough estimate of this effect, and of its observability by space based detectors like LISA.

A useful quantity to consider is the number of gravitational-wave cycles accumulated within a certain frequency band (see for instance Ref. [42]). This quan-

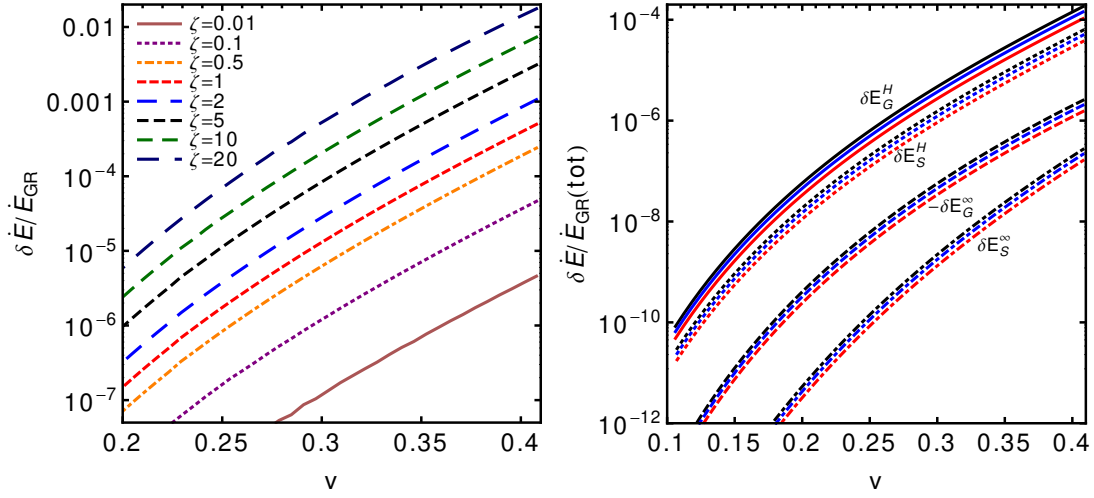


FIG. 1. (Color online) Left: Relative difference between the power emitted in gravitational waves in general relativity and DCS gravity, cf. Eq. (4.6), for different values of ζ . The sum is truncated at $\ell = 3$. The contribution in DCS gravity includes both the gravitational and the scalar fluxes, $\dot{E}_{\text{DCS}} = \dot{E}_{\text{grav}} + \dot{E}_{\text{scal}}$ at infinity and at the horizon. Right: Different contributions to the relative difference for different values of $\zeta = 0.5, 0.4, 0.3$, corresponding to different colors. The main contributions arise from the fluxes at the horizon and they are *positive*, whereas the difference in the gravitational flux at infinity is *negative*.

tity is defined as¹

$$\mathcal{N} = \int_{f_i}^{f_f} \frac{f}{\dot{f}} df, \quad (4.9)$$

with

$$f_i = \max(f_{\text{low}}, f_{1\text{yr}}), \quad (4.10)$$

$$f_f = \min(f_{\text{ISCO}}, f_{\text{up}}). \quad (4.11)$$

Here $f_{\text{low}} = 10^{-5}$ Hz and $f_{\text{up}} = 1$ Hz are two typical (lower and upper, respectively) cutoffs of the LISA noise curve, $f_{\text{ISCO}} = (6^{3/2}\pi M)^{-1}$ is the frequency at the ISCO. Finally, $f_{1\text{yr}}$ is the frequency of the gravitational radiation emitted one year before the coalescence (coalescence is for simplicity defined to occur when the particle reaches the ISCO). This choice is due to the fact that, despite the timespan of the LISA mission will likely be ~ 1 – 5 years, we make the most conservative assumption, considering one year of observation time. The frequency $f_{1\text{yr}}$ is obtained by solving

$$T_{\text{obs}} = \int_{f_{1\text{yr}}}^{f_{\text{ISCO}}} \frac{df}{\dot{f}} = 1 \text{ year}. \quad (4.12)$$

To solve Eqs. (4.9) and (4.12), one has to know how the particle is inspiralling into the massive BH. We use a simple prescription, the so-called adiabatic approximation,

in which the back-reaction is obtained by the energy flux, that is computed assuming that the particle moves on a geodesic orbit. Later in this Section we shall discuss this approach in more detail, assessing its accuracy; here we only remark that the error due to this approximation is much smaller than the other uncertainties in our problem (specifically the observation time, but also fundamental issues such as the magnitude of the coupling constants).

In order to compute $f_{1\text{yr}}$ using Eq. (4.12), one may consider a PN formula for \dot{f} . This choice has been widely adopted in previous works [26, 42, 43]. For EMRIs, the velocity during the latest stages before coalescence can be as large as a fraction of the speed of light and the PN approach may introduce sensible errors, as discussed in Appendix C. Therefore, we adopt a different prescription, as explained below. Our approach is well suited for the large-velocity and strong-field regime and thus it is expected to be more accurate for EMRIs. In Appendix C we compare it with other, less accurate, approaches.

We consider geodesic motion of a two-body system with masses m_1 and m_2 . The motion can be effectively reduced to that of a particle with reduced mass $\mu = m_1 m_2 / M = \eta M$ orbiting a central object with mass $M = m_1 + m_2$, consistently with the notation used in the previous sections. The frequency of gravitational waves emitted by the particle on a circular geodesic at $r = \bar{r}$ reads

$$f = \frac{\omega_K}{\pi} = \frac{1}{\pi} \sqrt{\frac{g'_{00}(\bar{r})}{2\bar{r}}} = \frac{1}{\pi} \sqrt{\frac{M}{\bar{r}^3}}, \quad (4.13)$$

from which we get $\dot{f} = -\frac{3}{2} f \frac{\dot{\bar{r}}}{\bar{r}}$. For a particle in a circular

¹ In this section f indicates the gravitational wave frequency, whereas, in the previous sections, it denoted the $\{t, t\}$ component of the metric (2.7). To avoid confusion while keeping the standard notation, in Eq. (4.13) this component is denoted by $g_{00}(r)$.

TABLE I. Corrections to the number of gravitational wave cycles accumulated within the frequency band $f \in [f_i, f_f]$ for some typical two-body systems. Data correspond to $T_{\text{obs}} = 1\text{yr}$ and are roughly fitted by Eq. (4.20).

M	$(1.4 + 10^4)M_\odot$		$(1.4 + 7 \times 10^5)M_\odot$		$(1.4 + 4 \times 10^6)M_\odot$		$(10 + 4 \times 10^6)M_\odot$		$(10 + 10^7)M_\odot$	
$f_i(\text{Hz})$	0.0205		0.0041		0.0010		0.00088		0.00040	
$f_f(\text{Hz})$	0.4396		0.0063		0.0011		0.00110		0.00044	
ζ	$-\delta\mathcal{N}$	$-\delta\mathcal{N}/\mathcal{N}$	$-\delta\mathcal{N}$	$-\delta\mathcal{N}/\mathcal{N}$	$-\delta\mathcal{N}$	$-\delta\mathcal{N}/\mathcal{N}$	$-\delta\mathcal{N}$	$-\delta\mathcal{N}/\mathcal{N}$	$-\delta\mathcal{N}$	$-\delta\mathcal{N}/\mathcal{N}$
20	38.2	3.78×10^{-5}	900	6.12×10^{-3}	455	1.40×10^{-2}	295	9.94×10^{-3}	179	1.38×10^{-2}
10	15.2	1.51×10^{-5}	365	2.48×10^{-3}	188	5.78×10^{-3}	121	4.07×10^{-3}	73.9	5.69×10^{-3}
5	6.28	6.21×10^{-6}	152	1.04×10^{-3}	79.5	2.44×10^{-3}	50.8	1.71×10^{-3}	31.2	2.40×10^{-3}
2	2.12	2.09×10^{-6}	51.7	3.51×10^{-4}	27.2	8.34×10^{-4}	17.3	5.82×10^{-4}	10.7	8.20×10^{-4}
1	0.98	9.70×10^{-7}	24.0	1.64×10^{-4}	12.7	3.89×10^{-4}	8.05	2.71×10^{-4}	4.97	3.82×10^{-4}
0.5	0.47	4.65×10^{-7}	11.5	7.85×10^{-5}	6.09	1.87×10^{-4}	3.87	1.30×10^{-4}	2.39	1.84×10^{-4}
0.4	0.37	3.69×10^{-7}	9.15	6.23×10^{-5}	4.83	1.48×10^{-4}	3.07	1.00×10^{-4}	1.89	1.45×10^{-4}
0.3	0.28	2.74×10^{-7}	6.81	4.63×10^{-5}	3.59	1.10×10^{-4}	2.28	7.68×10^{-5}	1.40	1.08×10^{-4}
0.2	0.18	1.81×10^{-7}	4.50	3.06×10^{-5}	2.37	7.29×10^{-5}	1.51	5.08×10^{-5}	0.93	7.17×10^{-5}
0.1	0.09	8.97×10^{-8}	2.23	1.52×10^{-5}	1.18	3.61×10^{-5}	0.75	2.52×10^{-5}	0.46	3.55×10^{-5}
0.01	0.009	8.95×10^{-9}	0.221	1.51×10^{-6}	0.12	3.61×10^{-6}	0.074	2.50×10^{-6}	0.046	3.53×10^{-6}

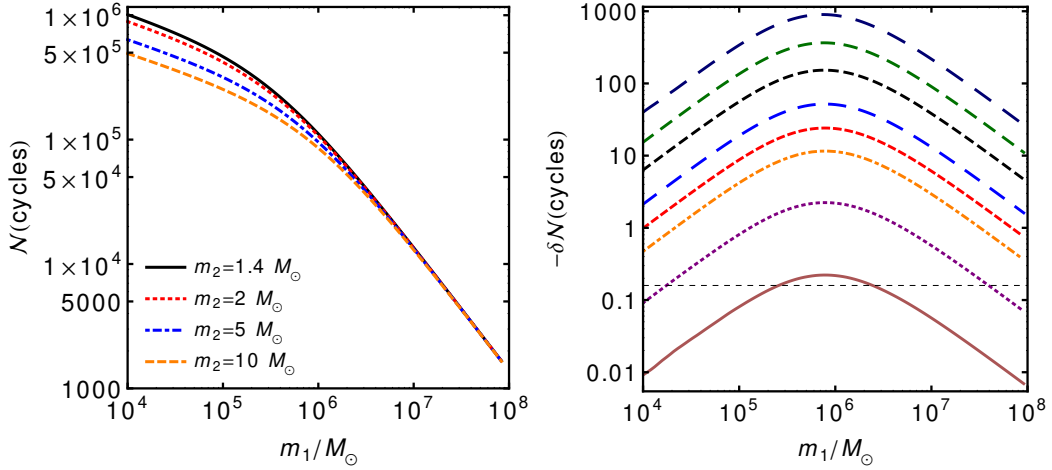


FIG. 2. (Color online) Left: Total number of cycles \mathcal{N} as a function of the central mass m_1 , for several values of m_2 , $T_{\text{obs}} = 1\text{yr}$ and $\zeta = 0.5$. Right: Corrections to the number of gravitational wave cycles accumulated during the inspiral of a small object ($m_2 = 1.4 M_\odot$) around a supermassive BH of mass m_1 in 1 year observation time before coalescence. We show $\delta\mathcal{N}$ as a function of m_1 for different values of ζ . Same legend as in Fig. 1

orbit we have

$$E_{\text{orb}} = \frac{\bar{r} - 2M}{\sqrt{\bar{r}(\bar{r} - 3M)}} \mu. \quad (4.14)$$

Putting all together, we find

$$\dot{f} = -\frac{3}{2} \frac{f}{\bar{r}} \frac{d\bar{r}}{dE_{\text{orb}}} \dot{E}_{\text{orb}}. \quad (4.15)$$

Finally, using Eq. (4.13) we get

$$\dot{f} = \frac{3}{\pi^{2/3} \mu M^{5/6}} \frac{[M^{1/3} f^{-2/3} - 3M\pi^{2/3}]^{3/2}}{[M^{1/3} f^{-2/3} - 6M\pi^{2/3}]} f^{2/3} \dot{E}_{\text{DCS}} \quad (4.16)$$

where $\dot{E}_{\text{DCS}} = \dot{E}_{\text{grav}} + \dot{E}_{\text{scal}} = -\dot{E}_{\text{orb}}$ is the total energy flux radiated away, using the standard flux balance equation

$$\dot{E}_{\text{orb}} + \dot{E}_{\text{grav}} + \dot{E}_{\text{scal}} = 0. \quad (4.17)$$

In the balance equation above, both the contributions at the horizon and at infinity must be taken into account.

We remark that we are modeling the EMRI orbit in the adiabatic approximation: the particle is in nearly geodesic motion, allowing to compute, at each time, the emitted energy flux \dot{E}_{DCS} assuming a geodesic orbit; furthermore, in this approach one assumes that the back-reaction is described by the flux balance (4.17). This approximation neglects the so-called “conservative part

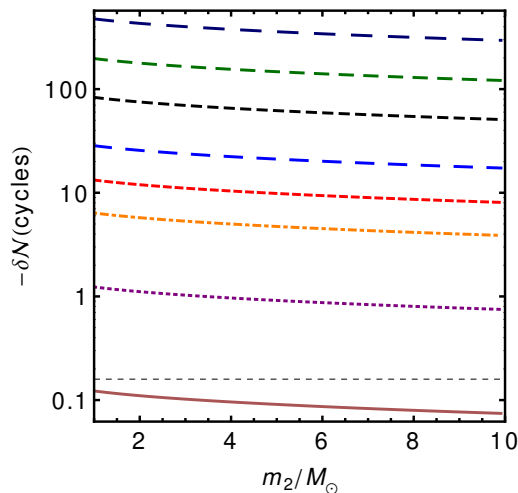


FIG. 3. (Color online) Correction to the number of gravitational wave cycles accumulated during the inspiral of a small object around a supermassive BH of mass $m_1 = 4 \times 10^6 M_\odot$ in 1 year observation time before coalescence, as a function of the mass m_2 of the small object and different values of ζ (same legend as in Fig. 1).

of the self-force”, which is a higher order effect contributing marginally to the gravitational signal (see Sec. 2 of [44]). Indeed, as shown in [45], for spinning BHs the conservative contribution can account for at most few cycles of the entire process, while for non-spinning BHs it contributes less than one radiant to a one year evolution [46]. Therefore, it may be necessary to take it into account in the data analysis of the process, but this effect can be neglected in assessing the relevance of DCS corrections for the EMRI signal.

Using the energy fluxes computed in the previous Section, we can therefore obtain the frequency at any instant prior to merger and the number of cycles \mathcal{N} left to merger. The total number of cycles is shown in the left panel of Fig. 2.

We can also compute the correction to the total number of cycles due to the CS coupling as follows. From the relation (4.16), we obtain $\delta\dot{f}/\dot{f} = \delta\dot{E}/\dot{E}_{GR}$, with $\delta X = X_{DCS} - X_{GR}$. Then, at first order,

$$\mathcal{N} = \int_{f_i}^{f_f} \frac{f}{\dot{f}} \left[1 - \frac{\delta\dot{E}}{\dot{E}_{GR}} \right] df, \quad (4.18)$$

and the correction in the number of cycles reads

$$\frac{\delta\mathcal{N}}{\mathcal{N}} = - \frac{\int_{f_i}^{f_f} \frac{f}{\dot{f}} \frac{\delta\dot{E}}{\dot{E}_{GR}} df}{\int_{f_i}^{f_f} \frac{f}{\dot{f}} df}. \quad (4.19)$$

The difference in the number of cycles is shown in Table I for different values of the CS coupling ζ and for a typical set of parameters.

The corrections depend on m_1 , m_2 and on the CS coupling ζ . This is shown in the right panel of Fig. 2

and in Fig. 3, where we indicate the fiducial threshold $\delta\mathcal{N} = (2\pi)^{-1}$ cycles (i.e. $\delta\Phi = 1$ rad) with a horizontal line. Corrections to general relativity are generally considered significant if they exceed one radiant over the observation time [47].

In the right panel of Fig. 3 we show the dependence on m_2 and on ζ for a central supermassive object with $m_1 = 4 \times 10^6 M_\odot$ (i.e., the mass of the supermassive BH at the center of the Milky Way [48]). Note that the dependence on m_2 appears to be very mild.

Overall, our results are well described by

$$\delta\mathcal{N} \sim -26\zeta \sqrt{\frac{M_\odot}{m_2}} \exp \left\{ -1.2 \log_{10}^2 \left[\frac{m_1}{m_{\max}} \right] \right\}, \quad (4.20)$$

where

$$m_{\max} = 6.6 \times 10^5 M_\odot \sqrt{\frac{m_2}{M_\odot}}, \quad (4.21)$$

is the location of the maximum in the left panel of Fig. 2 and it does not depend on the CS coupling. The fit above has been inspired by the curves in the left panel of Fig. 2. In a semi-logarithmic scale, these curves are approximately Gaussian, $y = y_0 \exp[a_0(x - x_m)^2]$, where y_0 , a_0 and x_m are the fit parameters and the expression (4.20) is simply written in the coordinate $x = \log_{10}(m_1)$. We estimate an error on the fit smaller than a few percent when $m_1 \in [10^5, 10^7] M_\odot$, $m_2 \in [1, 10] M_\odot$ and $\zeta \leq 1$. As shown in Fig. 4, for larger values of the CS coupling, $|\delta\mathcal{N}|$ grows faster than linearly as a function of ζ , and Eq. (4.20) would acquire higher order in ζ^2 contributions. For example when $\zeta \sim 20$, the fit (4.20) is accurate within 50%.

The presence of a maximum in $\delta\mathcal{N}(m_1)$ (Fig. 2, right panel) can be understood as follows: on one hand, the DCS correction for a given value of $\zeta = 16\pi\alpha^2/(\beta M^4)$ becomes more significant as $M = m_1 + m_2$ increases, as it appears from Eqs. (2.9)-(2.16); on the other hand, for large values of M the total number of cycles decreases (see Fig. 2, left panel), and thus $\delta\mathcal{N}$ decreases, too.

V. CONCLUSIONS

We have studied the gravitational wave emission by a small object on a quasi-circular geodesic around a static, spherically symmetric, massive BH, in the context of Dynamical Chern-Simons gravity. This process can describe for instance the inspiralling of a neutron star or stellar-mass BH into a supermassive BH, and is thought to occur frequently in the universe. In fact, EMRIs are one of the main preferred sources of gravitational waves for space-based detector LISA. We have shown that, because the stellar-size object spends many cycles in the bandwidth of LISA, the small effect of coupling to the DCS term “piles up” giving rise to measurable effects, in particular a decrease in the number of cycles over a fixed frequency bandwidth.

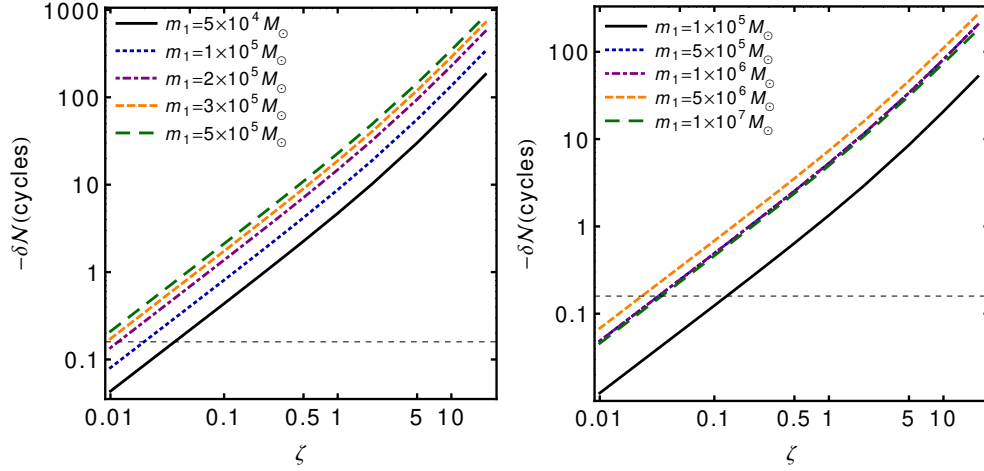


FIG. 4. (Color online) Correction to the number of gravitational wave cycles accumulated during the inspiral of a small object around a supermassive BH of mass m_1 in 1 year observation time before coalescence. Left: $\delta\mathcal{N}$ as a function of ζ for some values of m_1 and $m_2 = 1.4M_\odot$. Right: same with $m_2 = 10M_\odot$. The corrections are linear in ζ .

Extensions of this work are necessary before useful constraints to the theory can be obtained. In particular, the space of Schwarzschild BHs is a set of measure zero in the space of solutions: real BHs are most likely to be rotating. An extension of the present formalism and results to spinning BHs (for instance to the general class found in Ref. [49]) is highly desirable, but might have to wait for more powerful techniques or full-blown numerical simulations. Since the curvature invariants are higher close to rapidly spinning BHs and since the ISCO gets closer to the horizon, rapidly spinning BHs are a potentially very interesting tool to test DCS gravity. Furthermore, we have focused on circular orbits, but eccentricity may play an important role. The formalism we developed already allows for studies of eccentric EMRIs in DCS gravity. For eccentric orbits around rotating BHs much larger corrections due to the CS coupling are expected. Therefore, our results should be seen as a lower limit of DCS corrections to the EMRI gravitational-wave signal.

Finally, the results described in this paper are valid for any value of ζ . However, astrophysical observations already constrain the CS coupling [20]

$$\xi = \frac{16\pi\alpha^2}{\beta} \lesssim 10^{16}\text{km}^4. \quad (5.1)$$

Notice that α and β are the *physical* parameters entering the action (2.1), so that the constraints on ζ (for instance those possibly arising from a comparison between future observational data from LISA with Table I or Figs. 2-4) should always be converted into constraints on ξ , depending on the lengthscale of the system under consideration.

In this case, from the definition (2.19) and the constraint (5.1) we obtain that, for objects with mass $M \lesssim 10^4 M_\odot$, the CS coupling ζ may be larger than unit and our results show that in this case the CS coupling introduces large corrections, which are potentially detectable

and not already ruled out by previous constraints. However, the point-like approximation used in this paper is justified for EMRIs ($m_1/m_2 \sim 10^4$ or larger) whereas, for smaller values of the mass ratio the structure of the smaller object, and the details of its backreaction, should be taken into account.

ACKNOWLEDGMENTS

It is our pleasure to thank Nico Yunes and Emanuele Berti for enlightening conversations and Eric Poisson for useful correspondence. We also thank Kent Yagi, Leo Stein and Nico Yunes for sharing with us some of their preliminary results [41]. This work was supported by the *DyBHo-256667* ERC Starting Grant and by FCT - Portugal through PTDC projects FIS/098025/2008, FIS/098032/2008, CTE-AST/098034/2008 and CERN/FP/116341/2010.

Appendix A: Derivation of the perturbation equations

In this appendix we describe the derivation of the perturbation equations (2.9), (2.10) and (2.11) with source terms S_{RW} , S_S and S_Z respectively.

Let us start with some definitions. We denote the Regge-Wheeler (RW) function by Q and the Zerilli function by Z . $Y^{\ell m}$ are the usual scalar spherical harmonics, in term of which, following Refs. [32, 38] we define vector and tensor spherical harmonics as follows

$$\begin{aligned} X_A^{\ell m} &= \varepsilon_A^B Y_{|B}^{\ell m}, & U_{AB}^{\ell m} &= \Omega_{AB} Y^{\ell m}, \\ V_{AB}^{\ell m} &= Y_{|AB}^{\ell m} + \frac{\ell(\ell+1)}{2} \Omega_{AB} Y^{\ell m}, & W_{AB}^{\ell m} &= X_{(A|B)}^{\ell m} \end{aligned}$$

where $\Omega_{AB} = (1, \sin^2 \theta)$, a bar denotes the covariant derivative with respect to the metric Ω_{AB} , and ε_{AB} is the Levi-Civita tensor on the unit two-sphere. Hereafter capital roman indices run over the angular coordinates (θ, φ) , while lower-case roman indices run over t and r . We work in the frequency domain and all the quantities are intended as Fourier transforms of some time-dependent quantity, i.e. schematically $A(\omega, r) = \frac{1}{2\pi} \int dt \tilde{A}(t, r) e^{i\omega t}$. Finally we define $A' \equiv \partial A(\omega, r)/\partial r$.

odd parity perturbations read

$$i\omega h_1' + h_0'' + \frac{2i\omega}{r} h_1 - \frac{2(\lambda+1)r - 4M}{r^3 f} h_0 + \frac{96\pi M \alpha}{r^5} (r\eta - 2\Theta) = P_{\omega\ell m}^t(r), \quad (\text{A2})$$

$$-\omega^2 h_1 + i\omega h_0' - \frac{2i\omega}{r} h_0 + \frac{2\lambda f}{r^2} h_1 + \frac{96i\pi \alpha \omega M}{r^4} \Theta = P_{\omega\ell m}^r(r), \quad (\text{A3})$$

$$\frac{i\omega}{f} h_0 + f h_1' + \frac{2M}{r^2} h_1 = P_{\omega\ell m}(r), \quad (\text{A4})$$

where $\lambda = (\ell+2)(\ell-1)/2$ and the source terms are the Fourier transforms of

$$P^a(t, r) \equiv \frac{16\pi r^2}{\ell(\ell+1)} \int T^{aB} X_B^* d\Omega, \quad (\text{A5})$$

$$P(t, r) \equiv 16\pi r^4 \frac{(\ell-2)!}{(\ell+2)!} \int T^{AB} W_{AB}^* d\Omega. \quad (\text{A6})$$

The three equations above are not independent, due to the Bianchi identity

$$\partial_t P^t + \partial_r P^r + \frac{2}{r} P^r - \frac{2\lambda}{r^2} P = 0. \quad (\text{A7})$$

Defining the RW function as (notice the sign difference with respect to Ref. [22])

$$Q^{\ell m}(\omega, r) = -\frac{f(r)}{r} h_1^{\ell m}(\omega, r), \quad (\text{A8})$$

from Eqs. (A2)-(A4) we obtain the equation for axial parity perturbations (2.9), with source term given by

$$S_{RW}(\omega, r) = \frac{1}{2\pi} \int dt S_{RW}(t, r) e^{i\omega t}, \quad (\text{A9})$$

$$S_{RW}(t, r) = \frac{f}{r} \left[\frac{2}{r} \left(1 - \frac{3M}{r} \right) P - f \partial_r P + P^r \right]. \quad (\text{A10})$$

The perturbation equation for the scalar field can be computed replacing Eq. (A1) into Eq. (2.4) and linearizing it. Using Eq. (A3), we obtain Eq. (2.10) with source term given by

$$S_S(\omega, r) = \frac{1}{2\pi} \int dt S_S(t, r) e^{i\omega t}, \quad (\text{A11})$$

$$S_S(t, r) = -if(r) \frac{6\ell(\ell+1)\alpha M}{r^4 \beta \omega} P^r. \quad (\text{A12})$$

We note that this source term is entirely due to the CS coupling. The polar sector, instead, is unaffected by the CS coupling. Hence, the equation for polar perturbations (2.11) is the same as in general relativity with source term given by [32]:

1. Perturbation equations with a general source

In our perturbative approach, the spacetime metric is $g_{\mu\nu} = g_{\mu\nu}^{(0)} + h_{\mu\nu}$ where $g_{\mu\nu}^{(0)}$ is the Schwarzschild metric (2.7), and $h_{\mu\nu}$ is the metric perturbation. We decompose $h_{\mu\nu}$ in tensor spherical harmonics choosing the RW gauge, as in Ref. [22] where the perturbation equations without source were derived.

There are two families of perturbations, the odd (or axial) parity perturbations (in our gauge described by the functions $h_0^{\ell m}(\omega, r)$ and $h_1^{\ell m}(\omega, r)$), and the even (or polar) parity perturbations (in our gauge described by the functions $H_0^{\ell m}(\omega, r)$, $H_1^{\ell m}(\omega, r)$, $H_2^{\ell m}(\omega, r)$ and $K^{\ell m}(\omega, r)$). Moreover, we decompose the scalar field as

$$\vartheta(t, r, \theta, \varphi) = \int_{-\infty}^{\infty} d\omega \sum_{\ell m} \frac{\Theta^{\ell m}(\omega, r)}{r} Y^{\ell m}(\theta, \varphi) e^{-i\omega t}. \quad (\text{A1})$$

In the rest of the Appendix, we leave implicit the ω dependence and the ℓ and m indices, a sum over which is assumed. The relevant first order Einstein equations for

$$S_Z(\omega, r) = \frac{1}{2\pi} \int dt S_Z(t, r) e^{i\omega t}, \quad (\text{A13})$$

$$S_Z(t, r) = \frac{1}{(\lambda+1)\Lambda} \left\{ r^2 f \left(f^2 \frac{\partial}{\partial r} N^{tt} - \frac{\partial}{\partial r} N^{rr} \right) + r(\Lambda - f) N^{rr} + r f^2 N^b \right. \\ \left. - \frac{f^2}{r\Lambda} \left[\lambda(\lambda-1)r^2 + (4\lambda-9)Mr + 15M^2 \right] N^{tt} \right\} + \frac{2f}{\Lambda} N^r - \frac{f}{r} N^\sharp, \quad (\text{A14})$$

where $\Lambda = \lambda + 3M/r$ and we have defined

$$N^{ab} = 8\pi \int T^{ab} Y^{\ell m*} d\Omega, \quad N^a = \frac{16\pi r^2}{\ell(\ell+1)} \int T^{aA} Y_{|A}^{\ell m*} d\Omega, \quad (\text{A15})$$

$$N^b = 8\pi r^2 \int T^{AB} U_{AB}^{\ell m*} d\Omega, \quad N^\sharp = \frac{32\pi r^4}{(\ell-1)\ell(\ell+1)(\ell+2)} \int T^{AB} V_{AB}^{\ell m*} d\Omega, \quad (\text{A16})$$

2. Source term for point particle on geodesics

Here we work out the explicit source terms for a point particle moving on geodesics around a Schwarzschild BH (see e.g. Ref. [32]). Let us consider a point-like particle on a timelike geodesic with coordinates $z_p^\mu(\tau)$. The stress-energy tensor (in the time domain) is

$$T^{\mu\nu} = \mu \int \frac{d\tau}{\sqrt{-g}} u^\mu u^\nu \delta^4(x^\alpha - z_p^\alpha), \quad (\text{A17})$$

where μ is the mass of the particle, $\delta^4(x^\alpha - z_p^\alpha)$ is the four-dimensional Dirac delta, τ is the proper time and $u^\mu(\tau) = \dot{z}_p^\mu(\tau)$ is the four-velocity. The integral above can be explicitly computed:

$$T^{\mu\nu} = \mu \frac{u^\mu(t) u^\nu(t)}{r_p(t)^2 u^t(t)} \delta(r - r_p(t)) \delta(\cos \theta) \delta(\varphi - \varphi_p(t)).$$

We introduce the semi-latus rectum p and the eccentricity e , as orbital parameters. They are defined so that the periastron and apastron are at $r = pM/(1+e)$ and $r = pM/(1-e)$, respectively. In terms of these parameters, the energy and angular momentum per unit mass of a point particle are

$$\tilde{E}^2 = \frac{(p-2-2e)(p-2+2e)}{p(p-3-e^2)}, \\ \tilde{L}^2 = \frac{M^2 p^2}{p-3-e^2}, \quad (\text{A18})$$

and the four velocity reads

$$u^\mu = \left\{ \frac{\tilde{E}}{f}, \sqrt{\tilde{E}^2 - \tilde{V}^2}, 0, \frac{\tilde{L}}{r^2} \right\}, \quad (\text{A19})$$

where $\tilde{V}^2 = f \left(1 + \tilde{L}^2/r^2 \right)$.

For point-like particles on geodesics the time-dependent source terms (A10) and (A14) can be com-

puted explicitly. They read [32]

$$S_{RW}(t, r) = G_{RW}(t, r) \delta[r - r_p(t)] + F_{RW}(t, r) \delta'[r - r_p(t)], \quad (\text{A20})$$

$$S_Z(t, r) = G_Z(t, r) \delta[r - r_p(t)] + F_Z(t, r) \delta'[r - r_p(t)], \quad (\text{A21})$$

with

$$G_{RW}(t, r) = \frac{f^2}{r^3} \left[\frac{4}{r} \left(1 - \frac{3M}{r} \right) A + B \right], \\ F_{RW}(t, r) = -A \frac{f^3}{r^3}, \\ G_Z(t, r) = a Y^*(t) + b Y_{|\varphi}^*(t) + c U_{\varphi\varphi}^*(t) + d V_{\varphi\varphi}^*(t), \quad (\text{A22})$$

$$F_Z(t, r) = \frac{8\pi}{\lambda+1} \frac{f^2}{\Lambda} \frac{\tilde{V}^2}{\tilde{E}} Y^*(t),$$

where

$$A = 16\pi \frac{(\ell-2)!}{(\ell+2)!} \frac{\tilde{L}^2}{\tilde{E}} W_{\varphi\varphi}^{*\ell m}(t), \\ B = \frac{8\pi}{\lambda+1} \frac{\tilde{L}}{\tilde{E}} u^r X_{\varphi}^{*\ell m}(t), \\ a = \frac{8\pi}{\lambda+1} \frac{f^2}{r\Lambda^2} \left\{ \frac{6M}{r} \tilde{E} + \right. \\ \left. - \frac{\Lambda}{\tilde{E}} \left[\lambda+1 - \frac{3M}{r} + \frac{\tilde{L}^2}{r^2} \left(\lambda+3 - \frac{7M}{r} \right) \right] \right\}, \\ b = \frac{16\pi}{\lambda+1} \frac{\tilde{L}}{\tilde{E}} \frac{f^2}{r^2\Lambda} u^r, \quad c = \frac{8\pi}{\lambda+1} \frac{\tilde{L}^2}{\tilde{E}} \frac{f^3}{r^3\Lambda}, \\ d = -32\pi \frac{(\ell-2)!}{(\ell+2)!} \frac{\tilde{L}^2}{\tilde{E}} \frac{f^2}{r^3}. \quad (\text{A23})$$

In the above expressions, $Y(t)$, $X_A(t)$, $U_{AB}(t)$, $V_{AB}(t)$, $W_{AB}(t)$ denote the scalar, vector and tensor spherical harmonics evaluated at the angular position of the particle $\varphi_p(t)$; thus, $Y(t)$ is shorthand notation for

$Y^{\ell m}(\pi/2, \varphi_p(t))$, and the same holds for the other harmonics.

Since the orbital motion takes place in the equatorial plane, each spherical harmonic function is evaluated at $\theta_p = \pi/2$. An important consequence of this is that the source term for the Zerilli function vanishes when $\ell + m$ is odd, while the source term for the RW function vanishes when $\ell + m$ is even.

Finally, the source term for the scalar equation (A12) is

$$S_S(t, r) = G_S(t, r) \delta[r - r_p(t)], \quad (\text{A24})$$

where

$$G_S(t, r) = -if^2 \frac{96\pi\alpha M}{r^4\beta\omega} \frac{\tilde{L}}{\tilde{E}} \frac{\sqrt{\tilde{E}^2 - \tilde{V}^2}}{r_p^2(t)} X_\varphi^*(t). \quad (\text{A25})$$

Notice that S_S , at variance with S_{RW} and S_Z , does not contain derivatives of the Dirac delta. Note also that if the orbit is circular, $\tilde{E} = \tilde{V}$, thus $S_S = 0$. This can be traced back to Eq. (A12), and to the fact that $P^r \sim T^{r\mu} \sim u^r = 0$ for circular orbits.

3. Source describing a particle in circular orbit

All quantities in the previous section are considered in the frequency domain: they depend on r and ω , although the dependence on ω has often been left implicit. To compute the sources $S_Z(\omega, r)$ and $S_{RW}(\omega, r)$, one should first consider the time domain sources $S_Z(t, r)$, $S_{RW}(t, r)$, and then compute their Fourier transforms. This operation proceeds straightforwardly in the case of a circular orbit $r \equiv \bar{r}$. Indeed, we have

$$r_p(t) = \bar{r}, \quad \phi_p(t) = \omega_K t,$$

where the Keplerian frequency reads

$$\omega_K = \sqrt{\frac{M}{r^3}}. \quad (\text{A26})$$

Furthermore the geodesics energy, angular momentum and four-velocity respectively read

$$\begin{aligned} \tilde{E} &= \frac{r - 2M}{\sqrt{r(r - 3M)}} \\ \tilde{L} &= r \sqrt{\frac{M}{r - 3M}} \\ u^\mu &= \left(\sqrt{\frac{r}{r - 3M}}, 0, 0, \frac{1}{r} \sqrt{\frac{M}{r - 3M}} \right). \end{aligned} \quad (\text{A27})$$

Using the definitions above, the source terms (A20), (A21), (A24) reduce to

$$\begin{aligned} S_{RW}(t, r) &= G_{RW}(t, r) \delta(r - \bar{r}) + F_{RW}(t, r) \delta'(r - \bar{r}) \\ S_Z(t, r) &= G_Z(t, r) \delta(r - \bar{r}) + F_Z(t, r) \delta'(r - \bar{r}) \\ S_S(t, r) &= 0. \end{aligned} \quad (\text{A28})$$

The dependence on t comes from the tensor spherical harmonics. For instance Eq. (A22) now reads (hereafter we write explicitly the indexes ℓ, m)

$$G_Z^{\ell m}(t, r) = a Y^{*\ell m}(\theta_p(t), \phi_p(t)) + \dots \quad (\text{A29})$$

with

$$\begin{aligned} Y^{*\ell m}(\theta_p(t), \phi_p(t)) &= Y^{*\ell m}\left(\frac{\pi}{2}, 0\right) e^{-im\phi_p(t)} \\ &= Y^{*\ell m}\left(\frac{\pi}{2}, 0\right) e^{-im\omega_K t}. \end{aligned}$$

and similarly for the other terms in Eq. (A22). Hence, we can write $G_Z^{\ell m}(t, r)$ as a quantity which does not depend on t (conventionally we will indicate it with a hat) times $e^{-im\omega_K t}$:

$$G_Z^{\ell m}(t, r) = \hat{G}_Z^{\ell m}(r) e^{-im\omega_K t} \quad (\text{A30})$$

where

$$\hat{G}_Z^{\ell m}(r) = a Y^{*\ell m}\left(\frac{\pi}{2}, 0\right) + \dots, \quad (\text{A31})$$

The same can be done with all other quantities. Then, the Fourier transform gives:

$$\begin{aligned} G_Z^{\ell m}(\omega, r) &= \frac{1}{2\pi} \int_{-\infty}^{+\infty} dt \hat{G}_Z^{\ell m}(r) e^{-im\omega_K t} e^{i\omega t} \\ &= \hat{G}_Z^{\ell m}(r) \delta(\omega - m\omega_K), \end{aligned}$$

and the same holds for the other quantities. Therefore,

$$\begin{aligned} S_{RW}^{\ell m}(\omega, r) &= \delta(\omega - m\omega_K) \times \\ &\quad \left[\hat{G}_{RW}^{\ell m}(r) \delta(r - \bar{r}) + \hat{F}_{RW}^{\ell m}(r) \delta'(r - \bar{r}) \right], \end{aligned} \quad (\text{A32})$$

$$\begin{aligned} S_Z^{\ell m}(\omega, r) &= \delta(\omega - m\omega_K) \times \\ &\quad \left[\hat{G}_Z^{\ell m}(r) \delta(r - \bar{r}) + \hat{F}_Z^{\ell m}(r) \delta'(r - \bar{r}) \right]. \end{aligned} \quad (\text{A33})$$

Appendix B: Perturbative Green's function approach

In this Appendix we develop a perturbative Green's function approach to solve Eqs. (2.9)-(2.11). This approach is valid in the small coupling limit. We shall compare it with the general method (valid for any coupling) adopted in the main text. The perturbative approach can be useful for possible analytical calculations and it is also important as independent check for numerical results.

As long as the dimensionless CS coupling ζ (2.19) is small, Eqs. (2.9)-(2.11) can be solved by a perturbative scheme. Indeed, as we shall see, the Regge-Wheeler function and the scalar field are consistent with the ansatz

$$\begin{aligned} Q &= Q^{(0)} + \zeta Q^{(1)}, \\ \Theta &= \Theta^{(0)} + \zeta \Theta^{(1)}. \end{aligned} \quad (\text{B1})$$

The function $Q^{(0)}$ is the solution of the standard Regge-Wheeler equation in general relativity

$$\left[\frac{d^2}{dr_*^2} + \omega^2 - V_{RW}(r) \right] Q(r) = S_{RW}(r), \quad (\text{B2})$$

and can be solved by the Green's function approach, as in Section III A, by considering the particle source only:

$$Q^{(0)}(r) = \frac{Q_+(r)}{W_{RW}} \int_{-\infty}^r dr_* Q_- S_{RW} + \frac{Q_-(r)}{W_{RW}} \int_r^{+\infty} dr_* Q_+ S_{RW} \quad (\text{B3})$$

(note that the Green's function expression is linear in the source). The function $\Theta^{(0)}$ is the lowest order contribution (in the CS coupling) to the scalar field Θ . Its equation can be found replacing the ansatz (B1) in Eq. (3.6): at lowest order in ζ , it gives

$$\left[\frac{d^2}{dr_*^2} + \omega^2 - V_S \right] \Theta^{(0)} = S_S - f \frac{(\ell+2)!}{(\ell-2)!} \frac{6iM\alpha}{\omega r^5 \beta} Q^{(0)}, \quad (\text{B4})$$

where $S_S \sim \alpha/\beta$ is given in Eq. (A12) and V_S is Eq. (2.14) at order α . Defining an effective source term

$$\bar{S}_S(r) \equiv S_S - f \frac{(\ell+2)!}{(\ell-2)!} \frac{6iM\alpha}{\omega r^5 \beta} Q^{(0)}(r), \quad (\text{B5})$$

we can write the solution of (B4) as

$$\Theta^{(0)}(r) = \frac{1}{W_\Theta} \left[\Theta_+(r) \int_{-\infty}^r dr_* \Theta_- \bar{S}_S + \Theta_-(r) \int_r^{+\infty} dr_* \Theta_+ \bar{S}_S \right]. \quad (\text{B6})$$

Finally, if we denote the scalar field source in the Regge-Wheeler equation (at lowest order in ζ) as

$$\bar{S}_{RW}(r) \equiv \frac{96i\pi M \omega f}{r^5} \alpha \Theta^{(0)}(r), \quad (\text{B7})$$

we get that the main correction to the Regge-Wheeler function is

$$\zeta Q^{(1)} = \frac{1}{W_{RW}} \left[Q_+(r) \int_{-\infty}^r dr_* Q_- \bar{S}_{RW} + Q_-(r) \int_r^{+\infty} dr_* Q_+ \bar{S}_{RW} \right]. \quad (\text{B8})$$

Note that $\bar{S}_S \sim \alpha/\beta$, therefore $\Theta^{(0)} \sim \alpha/\beta$, and then $S_{RW} \sim \alpha \Theta^{(0)} \sim \zeta$, consistently with Eq. (B8).

At infinity and at the horizon, where the fluxes are computed, we get

$$\begin{aligned} Q(r_* \rightarrow \pm\infty) &= (Q^{(0)} + \zeta Q^{(1)})(r_* \rightarrow \pm\infty) \\ &= \frac{e^{\pm i\omega r_*}}{W_{RW}} \int_{-\infty}^{\infty} dr_* Q_{\mp} (S_{RW} + \bar{S}_{RW}). \end{aligned} \quad (\text{B9})$$

Even for circular orbits, $\bar{S}_{RW} \sim \Theta^{(0)}$ is defined throughout the entire spacetime, thus the evaluation of the integrals above is more involved than in general relativity, in which we simply have $S_{RW} \sim \delta(r - \bar{r})$ for a circular orbit. This makes the perturbative approach much more time-consuming than the non-perturbative approach.

It is straightforward to extract the quantities relevant to compute the fluxes, Eqs. (4.2) and (4.4). Indeed, by applying the same procedure explained in the main text, we can define $Q_{\pm}^{(0)\ell m}(\omega, r) = \bar{Q}_{\pm}^{(0)\ell m}(r) \delta(\omega - m\omega_K) e^{\pm i\omega r_*}$ with

$$\bar{Q}_{\pm}^{(0)\ell m}(r) = \frac{Q_{\pm}(r)}{W_{RW}} \left[\frac{Q_{\pm} \hat{G}_{RW}^{\ell m}}{f} - \left(\frac{Q_{\pm} \hat{F}_{RW}^{\ell m}}{f} \right)' \right]_{\bar{r}},$$

for $r \lesssim \bar{r}$ respectively. Then, from Eqs. (B5)-(B8) one can compute the quantities $\Theta_{\pm}^{(0)\ell m}(r)$, $\bar{S}_{RW}^{\ell m}(r)$, $Q_{\pm}^{(1)\ell m}(r)$, and finally the complete Regge-Wheeler function $Q_{\pm}^{\ell m} = Q_{\pm}^{(0)\ell m} + \zeta Q_{\pm}^{(1)\ell m}$ at infinity, which has the form

$$Q_{\pm}^{\ell m}(\omega) = \bar{Q}_{\pm}^{\ell m} \delta(\omega - m\omega_K) e^{\pm i\omega r_*}. \quad (\text{B10})$$

In the same way, the scalar field perturbation $\Theta_{\pm}^{(0)\ell m}(\omega) \equiv \Theta_{\pm}^{(0)\ell m}(\omega, r_* \rightarrow \pm\infty)$ has the form

$$\Theta_{\pm}^{(0)\ell m}(\omega) = \bar{\Theta}_{\pm}^{(0)\ell m} \delta(\omega - m\omega_K) e^{\pm i\omega r_*}. \quad (\text{B11})$$

Notice that $\Theta^{(0)} \sim \alpha/\beta$, so that the corresponding energy flux is $\mathcal{O}(\zeta)$, consistently with our expansion (B8). The contribution of $\zeta \Theta^{(1)}$ to the energy flux is $\mathcal{O}(\zeta^2)$ and it is neglected in this approximation.

a. Comparison between the perturbative and the non-perturbative approach

Comparing the perturbative method with the general approach discussed in the main text is important for two reasons. First, it gives an independent check of both methods. Second, it allows to assert the validity region of the perturbative approach. In Fig. 5 we compare the corrections to the total energy flux and to the number of cycles obtained by the two methods.

When $\zeta \ll 1$, the methods agree very well, confirming each other. For example, when $p \sim 6$, the emitted fluxes computed with the two methods agree within 0.1% or better for $\zeta \lesssim 0.3$, whereas they differ by $\sim (1\%, 5\%, 10\%, 50\%, 100\%)$ when $\zeta \sim (0.5, 1, 2, 10, 20)$, respectively. Remarkably, the perturbative approach is valid within a few percent up to $\zeta \sim 1$ whereas, for larger values of ζ , it gives an *overestimated* flux.

b. On the dominance of fluxes at the horizon in DCS theory

One of the curious results borne out of this study, with important consequences for the main observational

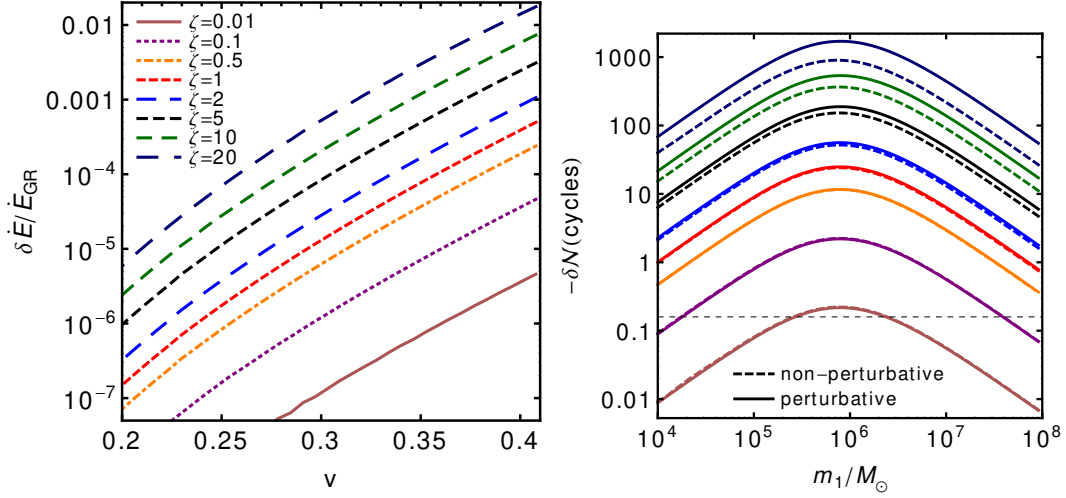


FIG. 5. (Color online) Comparison between the non-perturbative method described in the main text and the perturbative method described in Appendix B. Left: Corrections to the total flux emitted. Right: Corrections to the number of cycles for $m_2 = 1.4M_\odot$. In both panels, from below to top: $\zeta = 0.01, 0.1, 0.5, 1, 2, 5, 10, 20$. For $\zeta \gtrsim 1$ the perturbative method overestimates the total flux, resulting in a larger (in absolute value) correction to δN .

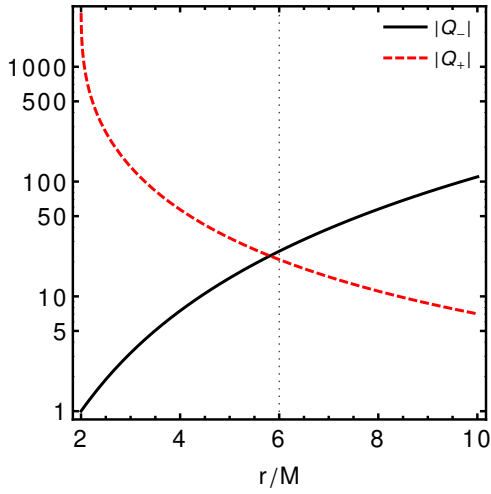


FIG. 6. (Color online) Homogeneous solutions of the Regge-Wheeler equation, $|Q_\pm|$.

prospects, concerns the fluxes at the horizon: while in general relativity fluxes at the horizon are orders of magnitude smaller than at infinity, this does not occur in DCS gravity; as summarized in Eqs. (4.8) the *corrections* imparted by the DCS coupling affect more strongly the flux at the horizon rather than at infinity. This can be understood from our perturbative analysis in the following way. From the above study, the axial Regge-Wheeler function in general relativity behaves as

$$\left| Q^{(0)}(r_* \rightarrow \pm\infty) \right| = \left| \frac{1}{W_{RW}} \int_{-\infty}^{+\infty} dr_* Q_{\mp} S_{RW} \right|. \quad (\text{B12})$$

We assume for simplicity circular orbits and that $S_{RW} \sim \delta(r - \bar{r})$, i.e. we neglect the $\delta'(r - \bar{r})$ contribution; however, this discussion can be easily generalized to non-circular orbits. The fluxes at the horizon and at infinity then depend on the value of the homogeneous solutions at $r = \bar{r}$. From Fig. 6 where we plot these homogeneous solutions, we see that, for $r > \bar{r} \geq 6M$,

$$|Q_+|^2 > |Q_-|^2, \quad (\text{B13})$$

which explains why the flux at the horizon is smaller than that at infinity. On the other hand, in this perturbative approach, the DCS correction to the Regge-Wheeler function behaves as

$$\left| \zeta Q^{(1)}(r_* \rightarrow \pm\infty) \right| = \left| \frac{1}{W_{RW}} \int_{-\infty}^{+\infty} dr_* Q_{\mp} \bar{S}_{RW} \right|. \quad (\text{B14})$$

Since $\bar{S}_{RW}(r) \sim \Theta^{(0)}/r^5$, the largest contribution comes from the near-horizon region $2M < r < 6M$, where (see Fig 6)

$$|Q_+|^2 < |Q_-|^2, \quad (\text{B15})$$

therefore the largest DCS correction to the flux is at the horizon.

Analogously, the DCS scalar field behaves as

$$\left| \Theta^{(0)}(r_* \rightarrow \pm\infty) \right| = \left| \frac{1}{W_{RW}} \int_{-\infty}^{+\infty} dr_* \Theta_{\mp} \bar{S}_S(r) \right|. \quad (\text{B16})$$

The homogeneous solutions of the scalar equation, Θ_{\pm} , are similar to the Regge-Wheeler homogeneous solutions Q_{\pm} ; in particular, close to the horizon one has $|\Theta_+|^2 < |\Theta_-|^2$, and $\bar{S}_S(r) \sim Q^{(0)}/r^5$, therefore the DCS scalar flux is larger at the horizon than at infinity.

Appendix C: Comparison of different ways to estimate the frequency one year prior to merger

In our calculation of the evolution of orbital frequency with time, we have adopted an adiabatic approximation, where the fluxes are determined numerically from those of a particle in geodesic motion. In the literature one sometimes finds other alternative calculations, with which we now compare our (more accurate) results.

One of the most common alternatives for estimating \dot{f} in Eqs. (4.9) and (4.12) consists in taking a PN approximation which, at 2PN level, reads [43]:

$$\dot{f} = \frac{96}{5\pi} \eta M^{5/3} (\pi f)^{11/3} \left[1 - \left(\frac{743}{336} + \frac{11}{4} \eta \right) (\pi M f)^{2/3} + 4\pi^2 M f + \left(\frac{34103}{18144} + \frac{13661}{2016} \eta + \frac{59}{18} \eta^2 \right) (\pi M f)^{4/3} \right], \quad (\text{C1})$$

(see e.g. Refs. [50, 51] for the 3.5PN formula). In the equation above, $M = m_1 + m_2$ is the total mass of the two-body system and $\eta = m_1 m_2 / M^2 = \mu / M$. Neglecting 2PN terms in Eq. (C1), we can solve Eq. (4.12) for $f_{1\text{yr}}$ analytically:

$$f_{1\text{yr}} = \frac{5^{3/8}}{2\sqrt{2}\pi M} \left(405 + 16\eta \frac{T_{\text{obs}}}{M} \right)^{-3/8}. \quad (\text{C2})$$

For example, from the formula above $f_{1\text{yr}} \sim 0.00274$ Hz for $T_{\text{obs}} = 1\text{yr}$, $m_1 = 10^6 M_\odot$ and $m_2 = 10 M_\odot$, while, including 2PN corrections, for the same parameters we obtain $f_{1\text{yr}} \sim 0.00252$ Hz, and including 3.5PN corrections [50, 51] we get $f_{1\text{yr}} \sim 0.00242$ Hz. Our own geodesic-based approach plus the numerical fluxes yields $f_{1\text{yr}} \sim 0.00223$ Hz. Notice also that, if we insert the quadrupole formula for the energy flux of a particle in a circular orbit,

$$\dot{E} \equiv \dot{E}_N = \frac{32}{5} \frac{\mu^2 M^3}{\bar{r}^5}, \quad (\text{C3})$$

in Eq. (4.16) and expand for $\bar{r}/M \gg 1$, then we recover the PN formula (C1) at first order.

The errors introduced by the PN approximation may be evaluated with a hybrid approach as follows. We compute the modification $\delta\mathcal{N}$ using the numerical flux \dot{E}_{DCS} in Eq. (4.19) but, in order to estimate the lower boundary of the integral (4.12), we use four different prescriptions: (i) \dot{f} is computed numerically within our geodesic-based approach, as explained in the main text; (ii) \dot{f} is given by its 3.5PN expansion (see Eq. (32) in Ref. [51]); (iii) \dot{f} is given by its 2PN expansion (C1); (iv) \dot{f} is given by the truncation of Eq. (C1) at Newtonian order. These different prescriptions affect the value of f_{in} and, in turn, Eq. (4.19).

This is shown in the left panel of Fig. 7. For large central masses, i.e. low frequencies, all the different prescriptions yield basically the same result to a good accuracy. For smaller central masses, we expect relativistic effects to become important: the system enters the LISA band when the small mass is already close to the ISCO, and where the PN expansion is less accurate. Indeed, in this regime the PN formula can give factors of order ~ 2 difference with respect to the more accurate prescription adopted in the main text.

As shown in the right panel of Fig. 7, similar deviations are observed also in general relativity. Indeed, if we compute \mathcal{N} from Eq. (4.9) using different prescriptions for f_{in} , we find that the number of cycles computed using the PN formula may be *overestimated* by $\sim 20\%$.

As discussed in Section IV B, the method based on the adiabatic approximation is better suited to deal with EMRIs. We note here that this is true not only in alternative theories like DCS gravity, but also in general relativity.

Appendix D: Expressions for the coefficients $C_\pm^{(i)}$ and $D_\pm^{(i)}$

The coefficients in Eqs. (3.13) and (3.14) depend solely on the solutions of the homogeneous system associated to Eq. (3.7) and their explicit forms read

$$\begin{aligned} C_+^{(1)} &= \Delta^{-1} \left[\Theta_-^{(2)} Q_-^{(1)} \Theta_+^{\prime(2)} - \Theta_+^{(2)} Q_-^{(1)} \Theta_-^{\prime(2)} - \Theta_-^{(1)} Q_-^{(2)} \Theta_+^{\prime(2)} + \Theta_+^{(2)} Q_-^{(2)} \Theta_-^{\prime(1)} + \Theta_-^{(1)} Q_+^{(2)} \Theta_-^{\prime(2)} - \Theta_-^{(2)} Q_+^{(2)} \Theta_-^{\prime(1)} \right], \\ C_+^{(2)} &= \Delta^{-1} \left[-\Theta_-^{(2)} Q_-^{(1)} \Theta_+^{\prime(1)} + \Theta_+^{(1)} Q_-^{(1)} \Theta_-^{\prime(2)} + \Theta_-^{(1)} Q_-^{(2)} \Theta_+^{\prime(1)} - \Theta_+^{(1)} Q_-^{(2)} \Theta_-^{\prime(1)} - \Theta_-^{(1)} Q_+^{(1)} \Theta_-^{\prime(2)} + \Theta_-^{(2)} Q_+^{(1)} \Theta_-^{\prime(1)} \right], \\ C_-^{(1)} &= \Delta^{-1} \left[\Theta_+^{(1)} Q_-^{(2)} \Theta_+^{\prime(2)} - \Theta_+^{(2)} Q_-^{(2)} \Theta_+^{\prime(1)} - \Theta_-^{(2)} Q_+^{(1)} \Theta_+^{\prime(2)} + \Theta_+^{(2)} Q_+^{(1)} \Theta_-^{\prime(2)} + \Theta_-^{(2)} Q_+^{(2)} \Theta_+^{\prime(1)} - \Theta_+^{(1)} Q_+^{(2)} \Theta_-^{\prime(2)} \right], \\ C_-^{(2)} &= \Delta^{-1} \left[-\Theta_+^{(1)} Q_-^{(1)} \Theta_+^{\prime(2)} + \Theta_+^{(2)} Q_-^{(1)} \Theta_+^{\prime(1)} + \Theta_-^{(1)} Q_+^{(1)} \Theta_+^{\prime(2)} - \Theta_+^{(2)} Q_+^{(1)} \Theta_-^{\prime(1)} - \Theta_-^{(1)} Q_+^{(2)} \Theta_+^{\prime(1)} + \Theta_+^{(1)} Q_+^{(2)} \Theta_-^{\prime(1)} \right] (\text{D1}) \end{aligned}$$

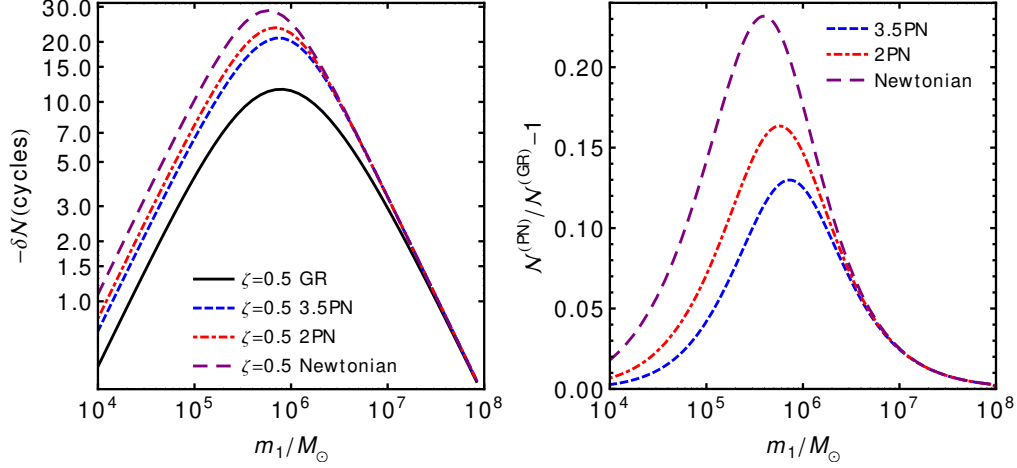


FIG. 7. (Color online) Left: Same as right panel of Fig. 2, but with different prescriptions to compute the frequency one year prior to merger. The first prescription (“GR”) is adopted in the main text and takes circular geodesic motion and the energy fluxes numerically computed in general relativity for a particle in circular orbit. The second (“3.5PN”) and third (“2PN”) prescriptions take respectively the 3.5PN formula [50, 51] and the 2PN formula, Eq. (C1) for the evolution of the frequency, while the third (“Newtonian”) is its truncation at lowest order. Right: relative difference between the total number of cycles in different approximations with respect to our geodesic-based approach for $\zeta = 0$ (general relativity). At low frequencies all prescriptions yield identical results, while at higher frequencies (smaller central masses), they can differ by a factor of order two.

and

$$\begin{aligned}
 D_+^{(1)} &= \Delta^{-1} \left[-\theta_+^{(2)} Q_-^{(1)} Q_-^{(2)} + \theta_-^{(2)} Q_-^{(1)} Q_+^{(2)} + \theta_+^{(2)} Q_-^{(2)} Q_-^{(1)} - \theta_-^{(1)} Q_-^{(2)} Q_+^{(2)} - \theta_-^{(2)} Q_+^{(2)} Q_-^{(1)} + \theta_-^{(1)} Q_+^{(2)} Q_-^{(2)} \right], \\
 D_+^{(2)} &= \Delta^{-1} \left[\theta_+^{(1)} Q_-^{(1)} Q_-^{(2)} - \theta_-^{(2)} Q_-^{(1)} Q_+^{(1)} - \theta_+^{(1)} Q_-^{(2)} Q_-^{(1)} + \theta_-^{(1)} Q_-^{(2)} Q_+^{(1)} + \theta_-^{(2)} Q_+^{(1)} Q_-^{(1)} - \theta_-^{(1)} Q_+^{(1)} Q_-^{(2)} \right], \\
 D_-^{(1)} &= \Delta^{-1} \left[-\theta_+^{(2)} Q_-^{(2)} Q_+^{(1)} + \theta_+^{(1)} Q_-^{(2)} Q_+^{(2)} + \theta_+^{(2)} Q_+^{(1)} Q_-^{(2)} - \theta_-^{(2)} Q_+^{(1)} Q_+^{(2)} - \theta_+^{(1)} Q_+^{(2)} Q_-^{(2)} + \theta_-^{(2)} Q_+^{(2)} Q_+^{(1)} \right], \\
 D_-^{(2)} &= \Delta^{-1} \left[\theta_+^{(2)} Q_-^{(1)} Q_+^{(1)} - \theta_+^{(1)} Q_-^{(1)} Q_+^{(2)} - \theta_+^{(2)} Q_+^{(1)} Q_-^{(1)} + \theta_-^{(1)} Q_+^{(1)} Q_+^{(2)} + \theta_+^{(1)} Q_+^{(2)} Q_-^{(1)} - \theta_-^{(1)} Q_+^{(2)} Q_+^{(1)} \right], \quad (D2)
 \end{aligned}$$

where

$$\begin{aligned}
 \Delta &= \theta_+^{(2)} \left[\theta_+^{(1)} Q_-^{(1)} Q_-^{(2)} - \theta_-^{(2)} Q_-^{(1)} Q_+^{(1)} - \theta_+^{(1)} Q_-^{(2)} Q_-^{(1)} + \theta_-^{(1)} Q_-^{(2)} Q_+^{(1)} \right] + \\
 &+ Q_+^{(1)} \left[\theta_-^{(2)} Q_-^{(1)} \theta_+^{(2)} - \theta_+^{(2)} Q_-^{(1)} \theta_-^{(2)} - \theta_-^{(1)} Q_-^{(2)} \theta_+^{(2)} + \theta_+^{(2)} Q_-^{(2)} \theta_-^{(1)} + \theta_-^{(1)} Q_+^{(2)} \theta_-^{(2)} - \theta_-^{(2)} Q_+^{(2)} \theta_-^{(1)} \right] + \\
 &+ Q_+^{(2)} \left[-\theta_-^{(2)} Q_-^{(1)} \theta_+^{(1)} + \theta_+^{(1)} Q_-^{(1)} \theta_-^{(2)} + \theta_-^{(1)} Q_-^{(2)} \theta_+^{(1)} - \theta_+^{(1)} Q_-^{(2)} \theta_-^{(1)} - \theta_-^{(1)} Q_+^{(1)} \theta_-^{(2)} + \theta_-^{(2)} Q_+^{(1)} \theta_-^{(1)} \right] + \\
 &- \theta_+^{(2)} Q_-^{(1)} Q_-^{(2)} \theta_+^{(1)} + \theta_+^{(2)} Q_-^{(1)} Q_+^{(1)} \theta_-^{(2)} + \theta_-^{(2)} Q_-^{(1)} Q_+^{(2)} \theta_+^{(1)} - \theta_+^{(1)} Q_-^{(1)} Q_+^{(2)} \theta_-^{(2)} + \theta_+^{(2)} Q_-^{(2)} Q_-^{(1)} \theta_+^{(1)} + \\
 &- \theta_+^{(2)} Q_-^{(2)} Q_+^{(1)} \theta_-^{(1)} - \theta_-^{(1)} Q_-^{(2)} Q_+^{(2)} \theta_+^{(1)} + \theta_+^{(1)} Q_-^{(2)} Q_+^{(2)} \theta_-^{(1)} \quad (D3)
 \end{aligned}$$

is a generalized Wronskian, it is constant by virtue of the homogeneous system, and therefore can be factored

out of the integrals in Eqs. (3.13) and (3.14). In the equations above a prime denotes derivative with respect to the tortoise coordinate r_* .

[1] P. Amaro-Seoane *et al.*, Class.Quant.Grav. **24**, R113 (2007), [astro-ph/0703495].

[2] B. F. Schutz, J. Centrella, C. Cutler and S. A. Hughes, 0903.0100.

- [3] C. F. Sopuerta, GW Notes, Vol. 4, p. 3-47 (2010), [1009.1402].
- [4] F. Ryan, Phys.Rev. **D52**, 5707 (1995).
- [5] S. Deser, R. Jackiw and S. Templeton, Phys.Rev.Lett. **48**, 975 (1982).
- [6] A. Lue, L.-M. Wang and M. Kamionkowski, Phys.Rev.Lett. **83**, 1506 (1999), [astro-ph/9812088].
- [7] R. Jackiw and S. Pi, Phys.Rev. **D68**, 104012 (2003), [gr-qc/0308071].
- [8] T. L. Smith, A. L. Erickcek, R. R. Caldwell and M. Kamionkowski, Phys.Rev. **D77**, 024015 (2008), [0708.0001].
- [9] J. Polchinski, *String theory. Vol. 2: Superstring theory and beyond*, Cambridge, UK: Univ. Pr. (1998) 531 p.
- [10] A. Ashtekar, A. Balachandran and S. Jo, Int.J.Mod.Phys. **A4**, 1493 (1989).
- [11] V. Taveras and N. Yunes, Phys.Rev. **D78**, 064070 (2008), [0807.2652].
- [12] S. Mercuri and V. Taveras, Phys.Rev. **D80**, 104007 (2009), [0903.4407].
- [13] M. Adak and T. Dereli, 0807.1832.
- [14] S. Weinberg, Phys.Rev. **D78**, 063534 (2008), [0805.3781].
- [15] J. Garcia-Bellido, M. Garcia-Perez and A. Gonzalez-Arroyo, Phys.Rev. **D69**, 023504 (2004), [hep-ph/0304285].
- [16] S. H. Alexander and J. Gates, S.James, JCAP **0606**, 018 (2006), [hep-th/0409014].
- [17] S. H.-S. Alexander, M. E. Peskin and M. M. Sheikh-Jabbari, Phys.Rev.Lett. **96**, 081301 (2006), [hep-th/0403069].
- [18] K. Konno, T. Matsuyama, Y. Asano and S. Tanda, Phys.Rev. **D78**, 024037 (2008), [0807.0679].
- [19] S. Alexander and N. Yunes, Phys.Rept. **480**, 1 (2009), [0907.2562].
- [20] N. Yunes and F. Pretorius, Phys. Rev. **D79**, 084043 (2009), [0902.4669].
- [21] C. F. Sopuerta and N. Yunes, Phys.Rev. **D80**, 064006 (2009), [0904.4501].
- [22] V. Cardoso and L. Gualtieri, Phys.Rev. **D80**, 064008 (2009), [0907.5008], erratum: ibid. **D81**, 089903 (2010).
- [23] C. Molina, P. Pani, V. Cardoso and L. Gualtieri, Phys.Rev. **D81**, 124021 (2010), [1004.4007].
- [24] J. Pons, E. Berti, L. Gualtieri, G. Miniutti and V. Ferrari, Phys.Rev. **D65**, 104021 (2002), [gr-qc/0111104].
- [25] P. Pani, E. Berti, V. Cardoso, Y. Chen and R. Norte, Phys.Rev. **D81**, 084011 (2010), [1001.3031].
- [26] A. Ohashi, H. Tagoshi and M. Sasaki, Prog.Theor.Phys. **96**, 713 (1996).
- [27] L. Barack and N. Sago, Phys. Rev. **D75**, 064021 (2007), [gr-qc/0701069].
- [28] S. L. Detweiler, Phys. Rev. **D77**, 124026 (2008), [0804.3529].
- [29] E. Poisson, Living Rev.Rel. **7**, 6 (2004), [gr-qc/0306052].
- [30] L. Barack, Class.Quant.Grav. **26**, 213001 (2009), [0908.1664].
- [31] T. Tanaka, Y. Mino, M. Sasaki and M. Shibata, Phys.Rev. **D54**, 3762 (1996).
- [32] K. Martel, Phys.Rev. **D69**, 044025 (2004), [gr-qc/0311017].
- [33] M. Davis, R. Ruffini, J. Tiomno and F. Zerilli, Phys.Rev.Lett. **28**, 1352 (1972).
- [34] Y. Fujii and K.-I. Maeda, *The Scalar-Tensor Theory of Gravitation*, Cambridge, UK: Univ. Pr. (2003) 256 p.
- [35] W. E. Boyce and R. C. DiPrima, *Elementary Differential Equations and Boundary Value problems*, Wiley Interscience. (1965).
- [36] L. C. Stein, N. Yunes and S. A. Hughes, 1012.3144.
- [37] E. Poisson, Phys. Rev. **D70**, 084044 (2004), [gr-qc/0407050].
- [38] K. Martel and E. Poisson, Phys.Rev. **D71**, 104003 (2005), [gr-qc/0502028].
- [39] C. Cutler, E. Poisson, G. Sussman and L. Finn, Phys.Rev. **D47**, 1511 (1993).
- [40] E. Poisson, Phys.Rev. **D52**, 5719 (1995), [gr-qc/9505030].
- [41] K. Yagi, L. Stein and N. Yunes, in preparation (2011).
- [42] E. Berti, A. Buonanno and C. M. Will, Phys.Rev. **D71**, 084025 (2005), [gr-qc/0411129].
- [43] L. Blanchet, T. Damour, B. R. Iyer, C. M. Will and A. Wiseman, Phys.Rev.Lett. **74**, 3515 (1995), [gr-qc/9501027].
- [44] J. Thornburg, GW Notes, Vol. 5, p. 3-53 (2011), [1102.3647].
- [45] E. Huerta and J. R. Gair, Phys.Rev. **D79**, 084021 (2009), [0812.4208].
- [46] N. Yunes, A. Buonanno, S. A. Hughes, M. Coleman Miller and Y. Pan, Phys.Rev.Lett. **104**, 091102 (2010), [0909.4263].
- [47] C. Cutler *et al.*, Phys.Rev.Lett. **70**, 2984 (1993), [astro-ph/9208005].
- [48] A. M. Ghez *et al.*, Astrophys. J. **689**, 1044 (2008), [0808.2870].
- [49] S. Vigeland, N. Yunes and L. Stein, 1102.3706.
- [50] L. Blanchet, T. Damour, G. Esposito-Farese and B. R. Iyer, Phys.Rev.Lett. **93**, 091101 (2004), [gr-qc/0406012].
- [51] A. Buonanno, G. B. Cook and F. Pretorius, Phys.Rev. **D75**, 124018 (2007), [gr-qc/0610122].